Joint Congestion Control and Routing Optimization: An Efficient Second-Order Distributed Approach

Jia Liu, *Member, IEEE,* Ness B. Shroff, *Fellow, IEEE,* Cathy H. Xia, and Hanif D. Sherali

***Abstract*—Distributed joint congestion control and routing optimization has received a significant amount of attention recently. To date, however, most of the existing schemes follow a key idea called the back-pressure algorithm. Despite having many salient features, the first-order subgradient nature of the back-pressure based schemes results in slow convergence and poor delay performance. To overcome these limitations, in this paper, we make a first attempt at developing a second-order joint congestion control and routing optimization framework that offers utility-optimality, queue-stability, fast convergence, and low delays. Our contributions in this paper are three-fold: i) we propose a new second-order joint congestion control and routing framework based on a primal-dual interior-point approach; ii) we establish utility-optimality and queue-stability of the proposed second-order method; and iii) we show how to implement the proposed second-order method in a distributed fashion.**

***Index Terms*—Second-order distributed algorithm, multi-hop routing, congestion control.**

I. Introduction

With the rapid integration of new applications and technologies, recent years have witnessed a growing challenge in making communication networks work more efficiently. To date, while there exists a large body of work on optimization-based dynamic joint congestion control and routing policy for both wireline and wireless networks (see, e.g., [1]–[5]), most of these schemes follow a key idea called the "back-pressure algorithm," which traces its roots to the celebrated paper [6]. The enduring popularity of the back-pressure algorithm is primarily due to: i) a provable throughput optimality, ii) elegant cross-layer extensions, and iii) a distributed dynamic queue-length differential based routing policy that stabilizes all queues in the network. Researchers have also uncovered a fundamental connection between the back-pressure based congestion control and the Lagrangian dual decomposition framework plus the subgradient method in classical nonlinear optimization theory [1], [3], where (scaled) queue-lengths play the role of Lagrangian dual variables and the queue-length updates correspond to subgradient directions. This enlightening insight has unified techniques that originated independently from control and optimization theory.

However, despite all the salient features, the subgradient nature of the back-pressure based congestion control and routing schemes turns out to be a factor that plagues their performance in practice. Being a first-order method (subgradients can be viewed as a first-order support of the dual function), back-pressure based joint congestion control and routing schemes neglect the curvature of the objective function contour, which is characterized by the eigenvalue condition number of the Hessian matrix that usually becomes increasingly ill-conditioned as the iterates approach an optimal solution [7]. Hence, it necessitates a small update in each iteration [1]–[4], [8], which subsequently slows down convergence and undermines the performance of optimization. This limitation motivates us to pursue a *second-order* design approach for distributed dynamic congestion control and routing. The fundamental rationale behind our approach is that, as in classical nonlinear optimization theory [7], by considering the second-order Hessian information in congestion control anid routing, we can expect to alleviate the inherent ill-conditioned behavior of first-order methods, thus leading to much faster convergence and hence better performance in practice.

However, developing a dynamic distributed second-order congestion control and routing policy is highly challenging and results in this area remain scarce. First, unlike the relatively obvious queue-length connection between the back-pressure based algorithms, it remains unclear how one can utilize the insights from existing second-order network optimization algorithms [9]–[12] to guide the design of an optimal dynamic congestion control and routing policy. The main challenge is that the existing work in [9]–[12] are "static" schemes that operate with average rates and only yield fixed allocation solutions, rather than dynamic policies that are able to evolve with time instants to dynamically allocate resources. Also, their connection to observable network state information (e.g., queue-length) is still missing. Second, after constructing a second-order scheme, it remains a difficult task to prove its utility-optimality and queue-stability (defined formally in Section III). This is because the incorporation of the second-order Hessian information significantly complicates the computational schemes and necessitates new theoretical approaches in performance analysis. Lastly, how to implement the developed second-order scheme in a distributed fashion (comparable to first-order methods) is still an open question. Similar to the second-order optimization algorithms in [9]–[12], one would have to face the challenges arising from decentralizing the Hessian and Laplacian matrix inverse computations.

Manuscript received March 26, 2014; revised December 14, 2014; and accepted February 24, 2015. This work has been supported in part by NSF grants CNS-1446582, CNS-1012700, IIS-0916440, ECCS-1232118, SES-1409214, CNS-1247830, and CNS-1343222.

Jia Liu and Ness B. Shroff are with the Department of Electrical and Computer Engineering, The Ohio State University, Columbus, OH, 43210 USA (e-mail: {liu.1736, shroff.11}@osu.edu).

Cathy H. Xia is with the Department of Integrated Systems Engineering, The Ohio State University, Columbus, OH, 43210 USA (e-mail: xia.52@osu.edu).

Hanif D. Sherali is with the Grado Department of Industrial and Systems Engineering, Virginia Tech, Blacksburg, VA, 24061 USA (e-mail: hanifs@vt.edu).

Digital Object Identifier xx.xxxx/XXXX.xxxx.xxxxx.

The key contribution of this paper is that, for the first time, we successfully develop a second-order joint congestion control and routing framework to address the aforementioned technical difficulties and establish an analytical foundation that offers fast convergence and high performance. The main results and technical contributions of this paper are as follows:

- We propose a fast-converging second-order joint congestion control and routing framework based on a *primal-dual* interior-point approach with a simple step-size control strategy, such that the resultant scheme is well-suited for implementation in practice. Our primal-dual approach exposes a deep connection between observable network state information and the primal-dual interior-point optimization theory, which itself is an active research field in operations research today (see, e.g., [13] for a survey).
- We establish the utility-optimality and queue-stability of the proposed second-order framework. Our theoretical analysis unveils the fundamental reason behind the fast convergence in the proposed second-order framework. Interestingly, our analytical results naturally lead to a utility-optimality and queue-length trade-off relationship governed by the *barrier parameter* of the interior-point method. We compare this trade-off relationship to those in first-order methods and contrast their similarities and differences, thus further advancing our understanding of both first- and second-order methods in network optimization theory.
- We suggest several approaches to implement the proposed second-order method in a *distributed* fashion. In particular, for the distributed dual Newton direction computation (the most challenging part in our second-order method), we propose a new Sherman-Morrison-Woodbury (SMW) based iterative approach. We show that, on a L-link network, the SMW-based approach obtains the *precise* solution in $2L$ iterations, rather than asymptotically as in [9]–[11].

Collectively, our results in this paper contribute to an exciting development of a cross-layer network control and optimization theory with second-order techniques. The remainder of this paper is organized as follows. In Section II, we review related works. Section III introduces the network model and problem formulation. Section IV presents the algorithm and performance analysis of our second-order scheme. Section V develops the principal components of the distributed computations. Section VI presents some numerical results, and Section VII concludes the paper.

II. Related Work

In this section, we review the state-of-the-art of both first- and second-order methods that are closely related to this paper. As mentioned earlier, there is a large body of work on first-order back-pressure based joint congestion control and routing (e.g., [1]–[4], [8], [14]) Among these works, the scheme in [3] is the most related and can be directly compared to our work since it is also a primal-dual based controller, where the primal and dual variables are updated jointly (hence relatively more convenient to implement in practice). Thanks to the second-order structure, our approach requires a much less conservative step-size selection, while achieving a steeper negative Lyapunov drift rate and inducing a much faster (three orders of magnitude numerically) convergence than in [3]. On the other hand, the schemes in [1], [2], [4] can be categorized as dual-based controllers, where an inner subproblem defined in terms of primal variables needs to be solved for each fixed set of dual variables. Thus, a counterpart of primal-dual step-size selection does not exist. However, similar Lyapunov drift rate analysis and numerical results also indicate a slow convergence performance due to their first-order nature.

In the second-order domain, recent (centralized and distributed) interior-point based methods for network optimization can be found in [10]–[12], [15]–[19]. In particular, significant efforts have been made to decentralize the second-order computations, including a Gaussian belief propagation technique in [16]–[18] and a matrix-splitting approach in [19] for flow control (with fixed routing); and a consensus-based local averaging scheme for minimum cost routing (with fixed source rates) in [12]. In our previous work [10], [11], we developed distributed second-order methods for cross-layer optimization (joint flow control, routing, and scheduling) in both wireline and wireless networks. However, all these second-order methods operate with *long-term rates* and do *not* consider queue evolution and stability. Moreover, they can be all categorized as the classical barrier interior-point approach. Different from these previous work, this paper is motivated by recent observations on the superior efficiency of the primal-dual interior-point approach compared to the barrier-based approach [13]. The main difference between the barrier interior-point approach and the primal-dual interior-point approach lies in different approaches in handling the so-called perturbed KKT system (cf. Eqs. (13)–(16) in the context of this paper). From the perspective of the perturbed KKT system handling, the barrier approach can be interpreted as a "restricted" version of the primal-dual approach (see [20, Page 611]). Moreover, it has been widely observed in practice that the barrier-based interior-point approach is less efficient than the primal-dual method [13], [20], which is due to the fact that the Newton-step obtained by the barrier-based approach tends to produce infeasible primal solutions (see [13, Sec. 4.3.3] for details). Therefore, the development of our primal-dual second-order method in this paper follows a more effective solution process. We also note that, recently, the authors of [21] have proposed a second-order distributed algorithm to accelerate the convergence of the back-pressure algorithm. Our work differs from [21] in the following key aspects. First, the algorithm in [21] only considers routing *without* addressing congestion control for end-to-end utility optimality. Second, the second-order acceleration in [21] is applied only in the dual domain to adjust back-pressure differentials, while the primal variables (routing decisions) are determined by the "soft backpressure" policy in [22], which is a waterfilling-type scheme for multiplexing different sessions on each link. The waterfilling level does not have a closed-form solution and has to be determined numerically. In contrast, our scheme adjusts both primal and dual variables by taking second-order Hessian information into consideration. In each time-slot, the multiplexing fraction of each session on each link naturally follows from the Hessian inverse, which

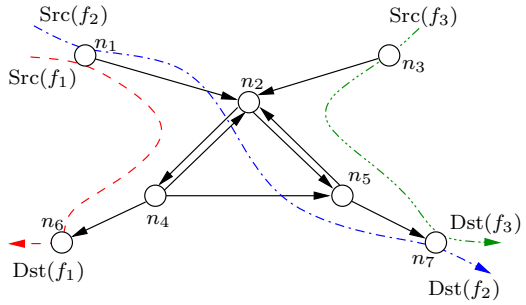

Fig. 1. An illustrative example of the network model.

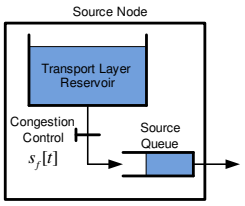

Fig. 2. An illustrative example of source node congestion control.

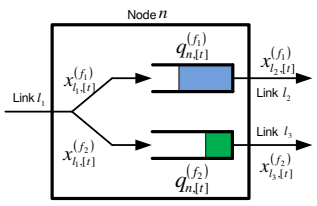

Fig. 3. An illustrative example of routing at an intermediate node.

can be determined in closed-form distributively (cf. Eq. (35)).

III. Network Model and Problem Formulation

We first introduce the notation style in this paper. We use boldface to denote matrices and vectors. We let $\mathbf{A}^T$ denote the transpose of $\mathbf{A}$. $\text{Diag}\{\mathbf{A}_1,\ldots,\mathbf{A}_N\}$ represents the block diagonal matrix with $\mathbf{A}_1,\ldots,\mathbf{A}_N$ on its main diagonal. We let $(\mathbf{A})_{ij}$ represent the entry in the i-th row and j-th column of $\mathbf{A}$ and let $(\mathbf{v})_m$ represent the m-th entry of $\mathbf{v}$. We let $\mathbf{I}_K$ denote the K-dimensional identity matrix, and let $\mathbf{1}_K$ and $\mathbf{0}_K$ denote the K-dimensional vectors whose elements are all ones and zeros ("K" may be omitted for brevity if the dimension is clear from the context). We let $\lambda_{\min}\{\mathbf{A}\}$ and $\lambda_{\max}\{\mathbf{A}\}$ denote the smallest and largest eigenvalues of $\mathbf{A}$, respectively.

Network model: We consider a time-slotted communication network system with time slot units being indexed by $t=0,1,2,\ldots$. As shown in Fig. 1, we represent the communication network by a directed graph $\mathcal{G}=\{\mathcal{N},\mathcal{L}\}$, where $\mathcal{N}$ and $\mathcal{L}$ are the sets of nodes and links, with $|\mathcal{N}|=N$ and $|\mathcal{L}|=L$, respectively. We assume that $\mathcal{G}$ is connected. There are F end-to-end sessions in the network, indexed by $f=1,\ldots,F$. Each session f has a source node and a destination node, represented by $\text{Src}(f),\text{Dst}(f)\in\mathcal{N}$, respectively. To avoid triviality, we assume that $\text{Src}(f)\neq\text{Dst}(f)$ for all f. The data of session f travel from $\text{Src}(f)$ to $\text{Dst}(f)$ through the network, possibly via multi-hop and multi-path routing.

Congestion control: As in [2], [3], we assume that the source node $\text{Src}(f)$ has a continuously-backlogged transport layer reservoir that contains session f's data, as illustrated in Fig. 2. Similar to a valve, in each time-slot t, a transport layer congestion controller determines the amount of data $s_{f,[t]}$ to be released from this reservoir into a network layer source queue, where the data awaits to be routed to node $\text{Dst}(f)$ through the network. In other words, $\{s_{f,[t]}\}$ acts as the arrival process to the source queue. To control the burstiness, we let $s_{f,[t]}\leq s_f^{\max},\forall t$. We let $\bar{s}_f\geq 0$ denote the time-average rate at which data of session f is injected at $\text{Src}(f)$ under congestion control, i.e., $\bar{s}_f=\lim_{T\to\infty}\frac{1}{T}\sum_{t=0}^{T-1}s_{f,[t]}$. Each session is associated with a utility function $U_f(\bar{s}_f)$, which represents the utility gained by session f when data is injected at rate $\bar{s}_f$. We assume that $U_f(\cdot)$ is strictly concave, monotonically increasing, and twice continuously differentiable.

Routing: We let $x_{l,[t]}^{(f)}\geq 0$ denote the rate offered to route session f's data in time-slot t at link l, as shown in Fig. 3. We let $\bar{x}_l^{(f)}\triangleq\lim_{T\to\infty}\frac{1}{T}\sum_{t=0}^{T-1}x_{l,[t]}^{(f)}$ represent the time-average routing rate of session f at link l. We use $\bar{\mathbf{s}}\triangleq[\bar{s}_1,\ldots,\bar{s}_F]^T$ and $\bar{\mathbf{x}}^{(f)}\triangleq[\bar{x}_1^{(f)},\ldots,\bar{x}_L^{(f)}]^T$ to group all congestion control and session f's routing rates. We denote the capacity of link l as C_l and assume that it is fixed, which is an appropriate model for wireline networks or wireless networks with orthogonal channels and fixed transmission power (see, e.g., [23], [24]). As in [1], [3], [25], we define the *network capacity region* as the largest set of congestion control rates $\bar{\mathbf{s}}$ such that there exists a routing policy for which the time-average routing rates $\{\bar{\mathbf{x}}^{(f)},\forall f\}$ satisfy the following constraints:

$$\sum_{l\in\mathcal{O}(n)}\bar{x}_l^{(f)}\geq\sum_{l\in\mathcal{I}(n)}\bar{x}_l^{(f)}+\bar{s}_f\mathbb{1}_f(n),\ \forall f,\forall n\neq\text{Dst}(f),\quad(1)$$

$$\sum_{f=1}^{F}x_{l,[t]}^{(f)}\leq C_l,\quad\forall l,t,\quad(2)$$

where $\mathcal{O}(n)$ and $\mathcal{I}(n)$ represent the sets of outgoing and incoming links at node n, respectively; $\mathbb{1}_f(n)$ is an indicator function that takes the value 1 if $n=\text{Src}(f)$ and 0 otherwise.

For convenience, we use a *node-arc incidence matrix* (NAIM) [26] $\mathbf{A}^{(f)}\in\mathbb{R}^{(N-1)\times L}$ and a *source vector* $\mathbf{b}^{(f)}\in\mathbb{R}^{N-1}$ to represent the network topology. Let $\text{Tx}(l)$ and $\text{Rx}(l)$ denote the transmitting and receiving nodes of link l, respectively. The entries $(\mathbf{A}^{(f)})_{nl}$ and $(\mathbf{b}^{(f)})_n$, $n\neq\text{Dst}(f)$, are defined as follows:

$$(\mathbf{A}^{(f)})_{nl}=\begin{cases}1 & \text{if } n=\text{Tx}(l),\\ -1 & \text{if } n=\text{Rx}(l),\\ 0 & \text{otherwise,}\end{cases}\quad(\mathbf{b}^{(f)})_n=\begin{cases}1 & \text{if } n=\text{Src}(f),\\ 0 & \text{otherwise.}\end{cases}$$

Then, the constraint in (1) can be compactly written as: $\mathbf{A}^{(f)}\bar{\mathbf{x}}^{(f)}-\bar{s}_f\mathbf{b}^{(f)}\geq\mathbf{0},\quad\forall f=1,2,\ldots,F.$

Queue-stability: We assume that each node maintains a separate queue for each session f, as shown in Fig. 3. We let $q_{n,[t]}^{(f)}\geq 0$ represent the amount of data in session f's queue at node n at time t. Since data leave the network upon reaching destinations, we have $q_{\text{Dst}(f),[t]}^{(f)}=0,\ \forall t$. The evolution of $q_{n,[t]}^{(f)}$, $n\neq\text{Dst}(f)$, is given by:

$$q_{n,[t+1]}^{(f)}=\left(q_{n,[t]}^{(f)}-\sum_{l\in\mathcal{O}(n)}x_{l,[t]}^{(f)}\right)^+\!+\sum_{l\in\mathcal{I}(n)}\widehat{x}_{l,[t]}^{(f)}+s_{f,[t]}\mathbb{1}_f(n),\quad(3)$$

where $(\cdot)^+\triangleq\max\{0,\cdot\}$ and $\widehat{x}_{l,[t]}^{(f)}$ is the *actual* routing rate. Note that $\widehat{x}_{l,[t]}^{(f)}\leq x_{l,[t]}^{(f)}$ since $\text{Tx}(l)$ may have less than $x_{l,[t]}^{(f)}$ amount of data to transmit. Let $\mathbf{q}_{[t]}\triangleq[q_{n,[t]}^{(f)},\forall f,\forall n\neq\text{Dst}(f)]^T$ group all queue lengths at time t. In this paper, we

adopt the following notion of queue-stability (same as in [3]): Under a congestion control and routing scheme, we say that the network is *stable* if the norm of steady-state queue-lengths remains finite, i.e., $\limsup_{t\to\infty} \|\mathbf{q}_{[t]}\| < \infty$.

Problem formulation: In this paper, our goal is to develop an optimal joint congestion control and routing scheme to maximize the total utility $\sum_{f=1}^{F} U_f(\bar{s}_f)$, subject to the network capacity region constraints and that the network is stable. Putting together the models presented earlier yields the following joint congestion control and routing (JCCR) optimization problem:

JCCR:

$$\begin{aligned}
\text{Maximize} \quad & \sum_{f=1}^{F} U_f(\bar{s}_f) \\
\text{subject to} \quad & 1)\ \mathbf{A}^{(f)}\bar{\mathbf{x}}^{(f)} - \bar{s}_f \mathbf{b}^{(f)} \geq \mathbf{0}, && \forall f, \\
& 2)\ \sum_{f=1}^{F} x_{l,[t]}^{(f)} \leq C_l, && \forall l, t, \\
& 3) \text{ Stability of all network queues,} \\
& 4)\ x_{l,[t]}^{(f)} \geq 0,\ \forall f, l, t; \quad s_{f,[t]} \geq 0,\ \forall f, t.
\end{aligned}$$

As mentioned earlier, several first-order schemes based on the back-pressure idea [6] have been proposed (e.g., [1]–[5]) to solve Problem JCCR. However, the convergence of these first-order schemes is slow, which could lead to poor performance in practice. In what follows, we will investigate a new second-order joint congestion control and routing framework.

IV. A Second-Order Congestion Control and Routing Optimization Framework

In Section IV-A, we first present our second-order joint congestion control and routing algorithm along with the main results on utility-optimality and queue-stability. Then, in Section IV-C, we explain the design rationale of our second-order approach. Section IV-D focuses on performance analysis and provides the proofs for the main theorems in Section IV-A. In Section IV-B, we discuss the key insights and intuition related to the results in Section IV-A.

A. The Algorithm and Main Theoretical Results

In this subsection, we present the main algorithm and associated theoretical results. First, we use $\mathbf{y}_{[t]}$ to denote all instantaneous *joint congestion control and routing decisions* at time t, which are arranged in the following link-based order: $\mathbf{y}_{[t]} \triangleq \left[s_{1,[t]} \cdots s_{F,[t]}, x_{1,[t]}^{(1)} \cdots x_{1,[t]}^{(F)}, \cdots, x_{L,[t]}^{(1)} \cdots x_{L,[t]}^{(F)}\right]^T$. We use $\mathbf{M} \triangleq \begin{bmatrix} \mathbf{B} & \mathbf{A}_1 & \cdots & \mathbf{A}_L \end{bmatrix}$ to group all *network topology* information, where $\mathbf{B}$ and $\mathbf{A}_l$ are defined as $\mathbf{B} \triangleq \text{Diag}\{\mathbf{b}^{(1)}, \ldots, \mathbf{b}^{(F)}\}$, and $\mathbf{A}_l \triangleq \text{Diag}\{-\mathbf{a}_l^{(1)}, \ldots, -\mathbf{a}_l^{(F)}\}$, and where in the definition of $\mathbf{A}_l$, the vector $\mathbf{a}_l^{(f)}$ is the l-th column of the matrix $\mathbf{A}^{(f)}$ in Problem JCCR (i.e., $\mathbf{A}^{(f)} = \left[\mathbf{a}_1^{(f)}, \mathbf{a}_2^{(f)}, \ldots, \mathbf{a}_L^{(f)}\right]$). Also, we let $\mathbf{N} \triangleq \text{Diag}\left\{\mathbf{0}_F^T, \mathbf{1}_F^T, \ldots, \mathbf{1}_F^T\right\} \in \mathbb{R}^{(L+1)\times(L+1)F}$ and $\mathbf{c} \triangleq [0, C_1, \ldots, C_L]^T \in \mathbb{R}^{L+1}$. Then, it can be verified that (1) and (2) can be compactly written as $\mathbf{M}\mathbf{y}_{[t]} \leq \mathbf{0}$ (in each time slot rather than on average) and $\mathbf{N}\mathbf{y}_{[t]} \leq \mathbf{c}$. Next, we define the following μ-scaled barrier augmented objective function:

$$\begin{aligned}
f_\mu(\mathbf{y}_{[t]}) \triangleq & -\mu \sum_{f=1}^{F} U_f(s_{f,[t]}) - \sum_{l=1}^{L} \log\left(C_l - \sum_{f=1}^{F} x_{l,[t]}^{(f)}\right) \\
& - \sum_{f=1}^{F} \log(s_{f,[t]}) - \sum_{l=1}^{L}\sum_{f=1}^{F} \log(x_{l,[t]}^{(f)}),
\end{aligned} \tag{4}$$

where $\mu > 0$ is called the *barrier parameter* (its meaning will be clear soon in Section IV-C). We let $\mathbf{g}_{[t]} \triangleq \nabla f_\mu(\mathbf{y}_{[t]})$ and $\mathbf{H}_{[t]} \triangleq \nabla^2 f_\mu(\mathbf{y}_{[t]})$ denote the gradient vector and Hessian matrix of $f_\mu(\cdot)$ evaluated at $\mathbf{y}_{[t]}$, respectively.

Next, we associate with Constraint (1) the dual variables $p_n^{(f)} > 0$, $\forall f$, $\forall n \neq \text{Dst}(f)$, which play the role of *prices* charged to session f for using node n. Accordingly, let $p_{n,[t]}^{(f)}$ be the price in time slot t. For convenience, we let $\mathbf{p}_{[t]} = [p_{n,[t]}^{(f)},\ \forall f, \forall n \neq \text{Dst}(f)]^T$ group all dual variables at time t and define a diagonal matrix $\mathbf{P}_{[t]} \triangleq \text{Diag}\left\{\mathbf{p}_{[t]}\right\}$.

Now, we define a diagonal matrix $\mathbf{Q}_{[t]} \triangleq \text{Diag}\left\{\mathbf{M}\mathbf{y}_{[t]}\right\}$ that reflects the *intended queue-length evolution* at time t. To see this, we can expand $\mathbf{M}\mathbf{y}_{[t]}$ to verify that each diagonal entry of $\mathbf{Q}_{[t]}$ is of the form: $-\sum_{l\in\mathcal{O}(n)} x_{l,[t]}^{(f)} + \sum_{l\in\mathcal{I}(n)} x_{l,[t]}^{(f)} + s_{f,[t]}\mathbb{1}_f(n)$, which is almost identical to the *actual* queue-length change in (3), except without the $(\cdot)^+$ projection and that all $\widehat{x}$-variables are replaced by x-variables. With this notation and given a strictly feasible initial solution at $t = 0$ (i.e., $\mathbf{M}\mathbf{y}_{[0]} < \mathbf{0}$, $\mathbf{N}\mathbf{y}_{[0]} < \mathbf{c}$, $\mathbf{p}_{[0]} > \mathbf{0}$), our second-order algorithm is illustrated in Algorithm 1.

In Algorithm 1, the primal variables $\mathbf{y}_{[t]}$ and dual variables $\mathbf{p}_{[t]}$ are updated following the (Newton) directions $\Delta\mathbf{y}_{[t]}$ in (5) and $\Delta\mathbf{p}_{[t]}$ in (6), respectively; both of which exploit not only the first-order gradient information $\mathbf{g}_{[t]}$, but also the second-order Hessian information $\mathbf{H}_{[t]}$, hence the name *second-order approach*. Also, the primal variables $\mathbf{y}_{[t]}$ and dual variables $\mathbf{p}_{[t]}$ are jointly updated in (7), thus being a *primal-dual* scheme. Compared to dual-based controllers (e.g., [1], [2], [4], [5], where a coupled subproblem defined in terms of primal variables is solved in each dual iteration), a primal-dual scheme is more convenient for implementation in practice. Note that Algorithm 1 is a dynamic policy that evolves with time instants and is based on the intended queue-length evolution $\mathbf{Q}_{[t]}$, which is an easily observable network state in practice. Moreover, as opposed to first-order methods where queue-length itself is directly used as a price, Eq. (6) shows that our pricing scheme exploits $\mathbf{Q}_{[t]}$, which corresponds to the intended *change of queue-length*. Therefore, the "change of queue-length" in our second-order method compared to the "queue-length value itself" in first-order backpressure methods can be viewed as one-order higher in the queue-length variation sense, hence providing another perspective to interpret the name "second-order." Lastly, the step-size control in (7) and (8) is used to ensure the utility-optimality result and will be further explained in Section IV-C. In (7) and (8), the parameter $M > 0$ could be set to some upper bound of the average source session rate to reduce the burstiness. The choice of the parameter ϵ will be addressed shortly in

Algorithm 1 A second-order joint congestion control and routing optimization algorithm (for a given μ).

1. In time-slot t, determine the *second-order* primal congestion control and routing and dual price (Newton) directions $\Delta\mathbf{y}_{[t]}$ and $\Delta\mathbf{p}_{[t]}$ as follows:

$$\Delta\mathbf{y}_{[t]} = -(\mathbf{H}_{[t]} - \mathbf{M}^T\mathbf{Q}_{[t]}^{-1}\mathbf{P}_{[t]}\mathbf{M})^{-1}(\mathbf{g}_{[t]} - \mathbf{M}^T\mathbf{Q}_{[t]}^{-1}\mathbf{1}), \quad (5)$$

$$\Delta\mathbf{p}_{[t]} = -(\mathbf{M}\mathbf{H}_{[t]}^{-1}\mathbf{M}^T - \mathbf{P}_{[t]}^{-1}\mathbf{Q}_{[t]})^{-1}\times [\mathbf{M}\mathbf{H}_{[t]}^{-1}(\mathbf{g}_{[t]} + \mathbf{M}^T\mathbf{p}_{[t]}) - (\mathbf{Q}_{[t]} + \mathbf{P}_{[t]}^{-1})\mathbf{1}]. \quad (6)$$

2. Update primal and dual variables *jointly* as:

$$\begin{bmatrix} \mathbf{y}_{[t+1]} \\ \mathbf{p}_{[t+1]} \end{bmatrix} = \left(\begin{bmatrix} \mathbf{y}_{[t]} \\ \mathbf{p}_{[t]} \end{bmatrix} + \pi \begin{bmatrix} \Delta\mathbf{y}_{[t]} \\ \Delta\mathbf{p}_{[t]} \end{bmatrix} \right)_{\mathcal{S}_\epsilon^M}, \quad (7)$$

where $\pi \in (0,1]$ is a constant step-size, and $(\cdot)_{\mathcal{S}_\epsilon^M}$ represents the projection onto the set $\mathcal{S}_\epsilon^M$ defined as:

$$\mathcal{S}_\epsilon^M \triangleq \left\{ (\mathbf{y},\mathbf{p}) \;\middle|\; \begin{array}{ll} \epsilon\mathbf{1} \le \mathbf{y} \le M\mathbf{1}, & \mathbf{M}\mathbf{y} \le -\epsilon\mathbf{1}, \\ \mathbf{N}\mathbf{y} \le \mathbf{c} - \epsilon\mathbf{1}, & \mathbf{p} \ge \epsilon\mathbf{1}. \end{array} \right\}, \quad (8)$$

where the constant $\epsilon > 0$ can be made arbitrarily close to zero and the constant $M > 0$ is used for burstiness reduction. Let $t \leftarrow t+1$ and go to Step 1.

Theorem 3 below. Note that, for ease of performance analysis in this section, the primal-dual Newton directions in (5) and (6) are expressed in matrix form for now. Their explicit distributed computational schemes will be derived later in Section V.

The following theorem says that the time-average congestion control rates and routing rates obtained under Algorithm 1 can be made *arbitrarily close* to the optimal solution by increasing the barrier parameter μ.

Theorem 1 (Utility-optimality)**.** *Let $\bar{\mathbf{y}}^*$ represent the optimal average rate solution to Problem JCCR. Under Algorithm 1 and for some given μ, if the step-size π scales as $O(\frac{1}{\mu})$, then there exists some constant $B \in (0,\infty)$ independent of μ such that $\limsup_{T\to\infty} \left|\frac{1}{T}\sum_{t=0}^{T-1}\mathbf{y}_{[t]} - \bar{\mathbf{y}}^*\right| \le \frac{B}{\sqrt{\mu}}$.*

For a time-varying positive definite matrix $\mathbf{A}_{[t]}$ (i.e., the smallest eigenvalue is strictly positive for all t), we let $\lambda_{\min}\{\mathbf{A}\} \triangleq \inf_t \left\{\lambda_{\min}\left\{\mathbf{A}_{[t]}\right\}\right\}$. The following result explains why Algorithm 1 enjoys a *fast* convergence.

Theorem 2 (Lyapunov drift rate)**.** *If $\bar{\mathbf{y}}$ is outside of $[\bar{\mathbf{y}}^* - \frac{B}{\sqrt{\mu}},\ \bar{\mathbf{y}}^* + \frac{B}{\sqrt{\mu}}]$, where $\bar{\mathbf{y}}^*$ and B are as defined in Theorem 1, then there is a negative Lyapunov drift that drives $\bar{\mathbf{y}}$ toward this interval, and the drift rate can be lower bounded by $R \triangleq \frac{\lambda_{\min}\{\mathbf{H}\}}{\lambda_{\min}\{\mathbf{H}-\mathbf{M}^T\mathbf{Q}^{-1}\mathbf{P}\mathbf{M}\}}$. Particularly, $R \ge 1$ as $\mu \to \infty$.*

Theorem 2 indicates that the second-order scaling term $(\mathbf{H}_{[t]} - \mathbf{M}^T\mathbf{Q}_{[t]}^{-1}\mathbf{P}_{[t]}\mathbf{M})^{-1}$ in (5) is crucial to the convergence of Algorithm 1. Without this term (replacing it by an identity matrix $\mathbf{I}$), we essentially "rediscover" a first-order back-pressure method (with $\mathbf{M}^T\mathbf{Q}_{[t]}^{-1}\mathbf{1}$ being the "pressure differential"). Thanks to this second-order scaling term, the "pulling force" of the negative Lyapunov drift is strong, allowing our scheme to approach the desired region *at least as fast as* at a rate R that is *insensitive* to the objective function contour.

TABLE I
PERFORMANCE SCALINGS COMPARISONS.

	2nd-order	1st-order (Primal-dual: [3])	1st-order (Dual: [2], [5])
Optimality gap	$O(\frac{1}{\sqrt{\mu}})$	$O(\frac{1}{\sqrt{V}})$	$O(\frac{1}{V})$
Queue-length	$O(\mu)$	$O(V)$	$O(V)$
Step-size	$O(\frac{1}{\mu})$	$O(\frac{1}{V^2})$	$O(\frac{1}{V})$

In contrast, the Lyapunov drift rate in first-order methods can be characterized by $\inf_t\{\lambda_{\min}\{\mathrm{Diag}\{-U_f''(s_{f,[t]}), \forall f\}\}\}$ (see, e.g., [3, Eq.(32)] and discussions thereafter), which is clearly sensitive to the objective function contour and could be very small (i.e., induce stalling). The next theorem states that, under Algorithm 1, the norm of steady-sate queue-lengths $\mathbf{q}_{[t]}$ remains finite, and hence inducing queue-stability.

Theorem 3 (Queue-stability)**.** *Under Algorithm 1 and for a given μ, letting $\epsilon = O(1/\mu)$, there exists a constant $K < \infty$ that scales as $O(\mu)$ such that $\limsup_{t\to\infty} \left\|\mathbf{q}_{[t]}\right\| \le K$.*

The proofs of Theorems 1, 2, and 3 will be given in Section IV-D. In what follows, we first discuss the performance scalings and the design rationale of Algorithm 1.

B. Performance Scalings of Algorithm 1

Similar to most first-order methods, Theorems 1 and 3 imply a trade-off between optimality gap and queue-length (hence delay). Specifically, although having a fundamentally different algorithmic meaning, the barrier parameter μ in our second-order method plays a similar role in characterizing the trade-off compared to the subgradient step-size scaling factor of the first-order methods (e.g., "V" in [2], "K" in [3], and β in [5]). Thus, we summarize the performance scalings of first- and second-order methods in Table I (all parameters in first-order methods are standardized to "V").

First, we see that all schemes have the same linear queue-length scaling. Second, the optimality gap scaling in [3] and our work are similar due to the common primal-dual nature. However, the $O(\frac{1}{\sqrt{V}})$-scaling in [3] is achieved at a slower convergence performance and under a more restrictive step-size scaling described next. For dual-based controllers in [2], [5], the optimality gap scales as $O(\frac{1}{V})$. Although this result appears to be better at first glance, a closer look reveals that such a direct comparison cannot be made. In [2], [5], the gap is measured by (in our notation) $\sum_f U_f(s_f^*) - \sum_f U_f(s_f)$, i.e., the gap of utility value. In contrast, Theorem 1 measures the gap by $\|\frac{1}{T}\sum_{t=0}^{T-1}\mathbf{y}_{[t]} - \bar{\mathbf{y}}^*\|$, i.e., the closeness to the optimal solution. For convenience, we let $\bar{\mathbf{y}} \triangleq \frac{1}{T}\sum_{t=0}^{T-1}\mathbf{y}_{[t]}$. As shown in Fig. 4, for an increasing strictly concave function $U(\cdot)$, even if $U(\bar{\mathbf{y}})$ is in order sense close to $U(\bar{\mathbf{y}}^*)$, it is still unclear how small $\|\bar{\mathbf{y}} - \bar{\mathbf{y}}^*\|$ is in general, and this distance could be large (e.g., if $U = \log(\cdot)$). In contrast, Theorem 1 directly characterizes $\|\bar{\mathbf{y}} - \bar{\mathbf{y}}^*\|$. Due to the concavity of $U(\cdot)$, a small $\|\bar{\mathbf{y}} - \bar{\mathbf{y}}^*\|$ guarantees a near-optimality in the objective value.

For step-size scaling, we can see that, for the first-order primal-dual scheme in [3] to approach optimality, the step-size should scale as $O(\frac{1}{V^2})$, which is *much smaller* than our $O(\frac{1}{\mu})$-scaling and implies a very slow convergence. For dual-based controllers [1], [2], [4], [5], although there is no direct

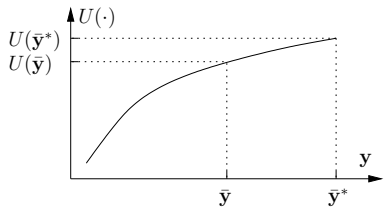

Fig. 4. Illustration of a monotonically increasing strictly concave utility function $U(\cdot)$ and the relationship between $|U(\bar{\mathbf{y}})-U(\bar{\mathbf{y}}^*)|$ and $\|\bar{\mathbf{y}}-\bar{\mathbf{y}}^*\|$.

primal-dual step-size counterpart, the dual step-size scaling therein can be understood as $O(\frac{1}{V})$, similar to our $O(\frac{1}{\mu})$. However, this $O(\frac{1}{V})$-scaling is obtained under the dual-based architecture, which is more cumbersome to implement due to the coupled inner primal subproblem.

Lastly, we remark that the $O(\frac{1}{\mu})$ step-size scaling is *not* restrictive in implementations since it is only a sufficient condition to establish Theorem 1. Given that the proof of Theorem 1 (see Section IV-D) is a limiting argument and the constant B in Theorem 1 may not be tight, the choice of the hidden constant in our $O(\frac{1}{\mu})$-scaling does not have to be small.

C. The Rationale behind the Algorithmic Design

Algorithm 1 is inspired by, and mirrors, a primal-dual interior-point method for directly solving Problem JCCR in terms of average rates $\bar{s}_f$ and $\bar{x}_l^{(f)}$. In what follows, we outline the main steps in our algorithmic design.

Step 1) A perturbed KKT system: As in standard interior-point methods [20], we first reformulate Problem JCCR by applying a logarithmic function to all inequality constraints and then accommodating them in the objective function to obtain the following *barrier* objective function (to be minimized):

$$\hat{f}_\mu^{(0)}(\bar{\mathbf{y}}) = -\sum_{f=1}^{F} U_f(\bar{s}_f) - \frac{1}{\mu}\sum_{l=1}^{L}\log\left(C_l - \sum_{f=1}^{F}\bar{x}_l^{(f)}\right) - \frac{1}{\mu}\sum_{f=1}^{F}\log(\bar{s}_f) - \frac{1}{\mu}\sum_{l=1}^{L}\sum_{f=1}^{F}\log(\bar{x}_l^{(f)}) - \frac{1}{\mu}\sum_{f=1}^{F}\sum_{n\neq \mathrm{Dst}(f)}\log\left(\sum_{l\in\mathcal{O}(n)}\bar{x}_l^{(f)} - \sum_{l\in\mathcal{I}(n)}\bar{x}_l^{(f)} - \bar{s}_f\mathbb{1}_f(n)\right),$$

Then, we can rewrite Problem JCCR as the following *unconstrained* optimization problem:

$$\textbf{R-JCCR: Minimize} \quad \hat{f}_\mu^{(0)}(\bar{\mathbf{y}}), \tag{9}$$

where, as $\mu\to\infty$, the original objective function of Problem JCCR dominates the barrier functions, and hence the solution of Problem R-JCCR approaches that of Problem JCCR asymptotically ([13], [20]). Next, we take the first derivatives of $\hat{f}_\mu^{(0)}(\bar{\mathbf{y}})$ and set them equal to zero (i.e., by way of the first-order Karush-Kuhn-Tucker (KKT) condition) to obtain:

$$\frac{\partial \hat{f}_\mu^{(0)}(\bar{\mathbf{y}})}{\partial \bar{s}_{(f)}} = -U'(\bar{s}_f) - \frac{1}{\mu\bar{s}_f} - \frac{1}{\mu}\Big(\sum_{l\in\mathcal{O}(\mathrm{Src}(f))}\bar{x}_l^{(f)} - \sum_{l\in\mathcal{I}(\mathrm{Src}(f))}\bar{x}_l^{(f)} - \bar{s}_f\Big)^{-1} = 0, \tag{10}$$

$$\frac{\partial \hat{f}_\mu^{(0)}(\bar{\mathbf{y}})}{\partial \bar{x}_l^{(f)}} = \frac{1}{\mu(C_l - \sum_{f'=1}^{F}\bar{x}_l^{(f')})} - \frac{1}{\mu x_l^{(f)}} - \frac{1}{\mu}\Big(\sum_{l\in\mathcal{O}(\mathrm{Tx}(l))}\bar{x}_l^{(f)} - \sum_{l\in\mathcal{I}(\mathrm{Tx}(l))}\bar{x}_l^{(f)} - \bar{s}_f\mathbb{1}_f(\mathrm{Tx}(l))\Big)^{-1} + \frac{1}{\mu}\Big(\sum_{l\in\mathcal{O}(\mathrm{Rx}(l))}\bar{x}_l^{(f)} - \sum_{l\in\mathcal{I}(\mathrm{Rx}(l))}\bar{x}_l^{(f)} - \bar{s}_f\mathbb{1}_f(\mathrm{Rx}(l))\Big)^{-1} = 0. \tag{11}$$

In (10) and (11), with respect to the final terms, we define dual variables (also called "barrier multipliers", see [13, Section 3.1]) as follows:

$$\hat{p}_n^{(f)} = \frac{1}{\mu\left(\sum_{l\in\mathcal{O}(n)}\bar{x}_l^{(f)} - \sum_{l\in\mathcal{I}(n)}\bar{x}_l^{(f)} - \bar{s}_f\mathbb{1}_f(n)\right)}. \tag{12}$$

Note that when $\bar{\mathbf{y}}$ is strictly primal feasible, we have $\hat{p}_n^{(f)}>0$. The purpose of introducing the $\hat{p}_n^{(f)}$-variables in (12) is to render a "perturbed KKT" system, which enables the subsequent queuing design and analysis. Toward this end, we use the vector $\widehat{\mathbf{p}} \triangleq [\hat{p}_n^{(f)}, \forall f, \forall n \neq \mathrm{Dst}(f)]^T$ to group all dual variables. Also, we let $\hat{f}_\mu(\bar{\mathbf{y}}) \triangleq \frac{1}{\mu}f_\mu(\bar{\mathbf{y}})$ (cf. (4) for the definition of $f_\mu(\cdot)$). Substituting (12) in (10) and (11) and then using $\hat{f}_\mu(\bar{\mathbf{y}})$, along with $\widehat{\mathbf{p}}$ and the property of $\mathbf{M}$, we arrive at the following *perturbed* KKT system that contains stationarity (ST), primal feasibility (PF), dual feasibility (DF), and perturbed complementary slackness (CS) conditions:

$$\begin{aligned}
&\text{(ST): } \nabla\hat{f}_\mu(\bar{\mathbf{y}}) + \mathbf{M}^T\widehat{\mathbf{p}} = 0,\\
&\text{(PF): } \bar{\mathbf{y}} > \mathbf{0}, \quad \mathbf{M}\bar{\mathbf{y}} < \mathbf{0},\\
&\text{(DF): } \widehat{\mathbf{p}} > \mathbf{0},\\
&\text{(CS): } -\mathrm{Diag}\{\mathbf{M}\bar{\mathbf{y}}\}\,\widehat{\mathbf{p}} = (1/\mu)\mathbf{1}.
\end{aligned}$$

Compared to the standard form of KKT conditions [7], the only difference in this perturbed KKT system is that the right-hand side (RHS) of the CS condition is changed from $\mathbf{0}$ to $\frac{1}{\mu}\mathbf{1}$. As a result, as $\mu\to\infty$, the perturbed KKT point $(\bar{\mathbf{y}},\widehat{\mathbf{p}})$ "almost" satisfies the standard KKT conditions, implying *near-optimality*. For more convenient algebraic derivations, we let $\mathbf{p}=\mu\widehat{\mathbf{p}}$ absorb the μ-factor and work with the following μ-scaled perturbed KKT system in the rest of the paper:

$$\begin{aligned}
&(\mu\text{-ST}): \nabla f_\mu(\bar{\mathbf{y}}) + \mathbf{M}^T\mathbf{p} = 0, && (13)\\
&(\mu\text{-PF}): \bar{\mathbf{y}} > \mathbf{0}, \quad \mathbf{M}\bar{\mathbf{y}} < \mathbf{0}, && (14)\\
&(\mu\text{-DF}): \mathbf{p} > \mathbf{0}, && (15)\\
&(\mu\text{-CS}): -\mathrm{Diag}\{\mathbf{M}\bar{\mathbf{y}}\}\,\mathbf{p} = \mathbf{1}. && (16)
\end{aligned}$$

Step 2) Second-order Newton's method: We will now apply *primal-dual-based* Newton's method (a second-order method) to determine a primal-dual pair $(\bar{\mathbf{y}},\mathbf{p})$ that satisfies the perturbed KKT conditions (13)–(16). Simply speaking, for our problem, the primal-dual Newton's method works as the following iterative search scheme starting from some initial feasible solution $(\bar{\mathbf{y}}^0,\mathbf{p}^0)$:

$$\begin{bmatrix}\bar{\mathbf{y}}^{k+1}\\ \mathbf{p}^{k+1}\end{bmatrix} = \begin{bmatrix}\bar{\mathbf{y}}^{k}\\ \mathbf{p}^{k}\end{bmatrix} + \pi^k\begin{bmatrix}\Delta\bar{\mathbf{y}}^{k}\\ \Delta\mathbf{p}^{k}\end{bmatrix}, \quad k\geq 0, \tag{17}$$

where π^k is a step-size; $\Delta\bar{\mathbf{y}}^k$ and $\Delta\mathbf{p}^k$ denote the primal and dual Newton directions, respectively.

We first work with the μ-ST and μ-CS conditions, while the μ-PF and μ-DF conditions will be handled later explicitly when determining the step-size. Note that finding a primal-dual pair $(\bar{\mathbf{y}}, \mathbf{p})$ that satisfies the μ-ST and μ-CS conditions amounts to computing the roots of a *nonlinear equality system* consisting of (13) and (16), which does not have analytic solutions in general and necessitates numerical methods. By using the Newton's method for root-finding [20], one can compute the Newton direction $[(\Delta\bar{\mathbf{y}}^k)^T,\ (\Delta\mathbf{p}^k)^T]^T$ as:

$$\begin{bmatrix} \mathbf{H}_k & \mathbf{M}^T \\ -\mathbf{P}_k\mathbf{M} & -\mathbf{Q}_k \end{bmatrix}\begin{bmatrix} \Delta\bar{\mathbf{y}}^k \\ \Delta\mathbf{p}^k \end{bmatrix}=-\begin{bmatrix} \mathbf{g}^k+\mathbf{M}^T\mathbf{p}^k \\ -(\mathbf{P}_k\mathbf{Q}_k+\mathbf{I})\mathbf{1} \end{bmatrix}, \quad (18)$$

where we let $\mathbf{g}^k \triangleq \nabla f_\mu(\bar{\mathbf{y}}^k)$, $\mathbf{H}_k \triangleq \nabla^2 f_\mu(\bar{\mathbf{y}}^k)$, $\mathbf{P}_k \triangleq \mathrm{Diag}\left\{\mathbf{p}^k\right\}$, and $\mathbf{Q}_k \triangleq \mathrm{Diag}\left\{\mathbf{M}\bar{\mathbf{y}}^k\right\}$. Note that, due to the perturbed KKT conditions, (18) is *different* from the Newton systems in existing second-order methods (cf. [9, Eq.(4)], [10, Eq.(8)], [11, Eq.(9)]). Also, directly solving (18) is undesirable due to its complex structure. A better way for solving (18) is to derive a reduced linear system by Gaussian elimination to obtain (assuming $\mathbf{p}^k > \mathbf{0}$ and hence $\mathbf{P}_k$ is non-singular, which can be ensured by the step-size control described next):

$$\Delta\bar{\mathbf{y}}^k = -\left(\mathbf{H}_k - \mathbf{M}^T\mathbf{Q}_k^{-1}\mathbf{P}_k\mathbf{M}\right)^{-1}(\mathbf{g}^k - \mathbf{M}^T\mathbf{Q}_k^{-1}\mathbf{1}), \quad (19)$$

$$\Delta\mathbf{p}^k = -\left(\mathbf{M}\mathbf{H}_k^{-1}\mathbf{M}^T - \mathbf{P}_k^{-1}\mathbf{Q}_k\right)^{-1} \times \left[\mathbf{M}\mathbf{H}_k^{-1}(\mathbf{g}_k + \mathbf{M}^T\mathbf{p}^k) - (\mathbf{Q}_k + \mathbf{P}_k^{-1})\mathbf{1}\right]. \quad (20)$$

Now, it is not difficult to recognize the structural similarity between (5)–(6) and (19)–(20).

Next, we handle the μ-PF and μ-DF conditions by step-size control. In standard primal-dual interior-point methods [13], the step-size control is based on *two* rules: The first one is to satisfy primal-dual feasibility by finding:

$$\pi^k = \max\left\{\pi \in [0,1] \;\middle|\; \begin{array}{l} \bar{\mathbf{y}}^k + \pi\Delta\bar{\mathbf{y}}^k \geq \epsilon\mathbf{1}, \\ \mathbf{M}(\bar{\mathbf{y}}^k + \pi\Delta\bar{\mathbf{y}}^k) \leq -\epsilon\mathbf{1}, \\ \mathbf{N}(\bar{\mathbf{y}}^k + \pi\Delta\bar{\mathbf{y}}^k) \leq \mathbf{c} - \epsilon\mathbf{1}, \\ \mathbf{p}^k + \pi\Delta\mathbf{p}^k \geq \epsilon\mathbf{1}, \end{array}\right\}, \quad (21)$$

where $\epsilon > 0$ is some arbitrarily small constant. Note that a full Newton step is taken if $\pi^k = 1$. The second step-size selection rule is to guarantee a *decreasing residual*: Let $\mathbf{r}_\mu(\bar{\mathbf{y}}^k, \mathbf{p}^k) \triangleq [(\mathbf{g}^k + \mathbf{M}^T\mathbf{p}^k)^T,\ (-\mathbf{P}_k\mathbf{Q}_k\mathbf{1} - \mathbf{1})^T]^T$ be the residual of μ-ST and μ-CS at $\bar{\mathbf{y}}^k$ (i.e., the right-hand side (RHS) of (18)). The second rule is to choose π^k to satisfy [13]:

$$\|\mathbf{r}_\mu(\bar{\mathbf{y}}^{k+1}, \mathbf{p}^{k+1})\| < \|\mathbf{r}_\mu(\bar{\mathbf{y}}^k, \mathbf{p}^k)\|. \quad (22)$$

Under the step-size rules in (21) and (22), the second-order convergence speed analysis follow from standard primal-dual interior-point methods (see [13, Chap. 5] and [27]).

Step 3) Back to Algorithm 1: Now, we can see that Algorithm 1 indeed mimics the foregoing approach to adjust $\mathbf{y}_{[t]}$ in *every time-slot*, rather than the average rate $\bar{\mathbf{y}}^k$. Moreover, Algorithm 1 has a much simplified step-size selection rule: We do *not* require a delicate line search to determine π^k as in (21) and have the residuals $\mathbf{r}_\mu(\bar{\mathbf{y}}^k, \mathbf{p}^k)$ decrease as in (22), both of which are expensive to check due to a large number of gradient and constraint evaluations in each time-slot. Rather, we use a fixed step-size $\pi \in (0, 1]$ and a projection to maintain primal-dual feasibility (a basic requirement in an interior-point method). Surprisingly, even with this much simplified and relaxed step-size rule, we are still able to show that the time-average of $\{\mathbf{y}_{[t]}, \mathbf{p}_{[t]}\}_{t=0}^{\infty}$ converges to a bounded region around the optimal solution as indicated in Theorem 1, which is *exactly the goal* of Problem JCCR.

D. Proofs of the Main Theorems

In this section, we provide (sketched) proofs for the theorems in Section IV-A for better readability. More detailed proof derivations can be found in the appendices.

Sketch of the proof of Theorem 1. The main idea and key steps for proving Theorem 1 are as follows. First, we consider the one-slot drift of the following particular choice of quadratic Lyapunov function:

$$V\left(\mathbf{y}_{[t]}, \mathbf{p}_{[t]}\right) \triangleq \frac{1}{2\pi}\left\|\mathbf{y}_{[t]} - \bar{\mathbf{y}}^*\right\|^2 + \frac{1}{2\mu^3\pi}\left\|\mathbf{p}_{[t]} - \mathbf{p}^*\right\|^2,$$

which can be interpreted as measuring the (unscaled) distance between a primal-dual iterate $(\mathbf{y}_{[t]}, \mathbf{p}_{[t]})$ and a perturbed KKT point $(\bar{\mathbf{y}}^*, \mathbf{p}^*)$ satisfying (13)–(16). For simplicity, we let $\mathbf{F}_{[t]}$ and $\mathbf{G}_{[t]}$ be defined as follows: $\mathbf{F}_{[t]} \triangleq \mathbf{H}_{[t]} - \mathbf{M}^T\mathbf{Q}_{[t]}^{-1}\mathbf{P}_{[t]}\mathbf{M}$ and $\mathbf{G}_{[t]} \triangleq \mathbf{M}\mathbf{H}_{[t]}^{-1}\mathbf{M}^T - \mathbf{P}_{[t]}^{-1}\mathbf{Q}_{[t]}$. Then, after some algebraic derivations and upper-bounding (see Appendices A-A and A-B for detailed derivations), we obtain the following relationship:

$$\Delta V\left(\mathbf{y}_{[t]}, \mathbf{p}_{[t]}\right) \triangleq V\left(\mathbf{y}_{[t+1]}, \mathbf{p}_{[t+1]}\right) - V\left(\mathbf{y}_{[t]}, \mathbf{p}_{[t]}\right) \leq -R\|\mathbf{y}_{[t]} - \bar{\mathbf{y}}^*\|^2 + \pi B_1 + \frac{1}{\mu}B_2 + \frac{1}{\mu}B_3, \quad (23)$$

where $R \triangleq \frac{\lambda_{\min}\{\mathbf{H}\}}{\lambda_{\min}\{\mathbf{F}\}} > 0$ (see Eq. (55) in Appendix A-A for detailed derivations) and B_1, B_2, and B_3 are some positive constants as defined in (59), (69), and (72) in Appendix A, respectively. Also, based on (59), (69), and (72) in Appendix A, we can conclude that B_1, B_2, and B_3 are independent of μ. It can be seen from (23) that if $\pi = O(1/\mu)$, we have $V(\mathbf{y}_{[t+1]}, \mathbf{p}_{[t+1]}) - V(\mathbf{y}_{[t]}, \mathbf{p}_{[t]}) \leq -R\|\mathbf{y}_{[t]} - \bar{\mathbf{y}}^*\|^2 + \frac{1}{\mu}\widehat{B}$, where $\widehat{B} \triangleq \alpha B_1 + B_2 + B_3$ for some $\alpha > 0$. Telescoping T via one-slot drift expressions for $t = 0, \ldots, T-1$ yields: $V\left(\mathbf{y}_{[T]}, \mathbf{p}_{[T]}\right) - V\left(\mathbf{y}_{[0]}, \mathbf{p}_{[0]}\right) \leq -R\sum_{t=0}^{T-1}\|\mathbf{y}_{[t]} - \bar{\mathbf{y}}^*\|^2 + \frac{T}{\mu}\widehat{B}$. Next, dividing both sides by TR, rearranging terms, and taking T to infinity, we have $\limsup_{T\to\infty}\frac{1}{T}\sum_{t=0}^{T-1}\|\mathbf{y}_{[t]} - \bar{\mathbf{y}}^*\|^2 \leq \frac{B^2}{\mu}$, where we let $B^2 \triangleq \widehat{B}/R$. Then, the proof is complete because when T is large, we have

$$\left|\frac{1}{T}\sum_{t=0}^{T-1}\left(\mathbf{y}_{[t]} - \bar{\mathbf{y}}^*\right)\right| \overset{(a)}{\leq} \left(\frac{1}{T}\sum_{t=0}^{T-1}\|\mathbf{y}_{[t]} - \bar{\mathbf{y}}^*\|^2\right)^{\frac{1}{2}} \leq \frac{B}{\sqrt{\mu}},$$

where inequality (a) follows from the triangular inequality and the basic relationship between l_1- and l_2-norms. We note that the most challenging step in the proof lies in the one-slot drift analysis, where we repeatedly exploit the key relationships in the perturbed KKT system in (13)–(16). We relegate the derivation details to Appendix A. □

Proof of Theorem 2. First, from (23), we have that the drift rate R is given by:

$$R \triangleq \frac{\lambda_{\min}\{\mathbf{H}\}}{\lambda_{\min}\{\mathbf{F}\}} = \frac{\inf_t\{\lambda_{\min}\{\mathbf{H}_{[t]}\}\}}{\inf_t\{\lambda_{\min}\{\mathbf{F}_{[t]}\}\}}.$$

Recall that $\mathbf{F}_{[t]}$ is defined as $\mathbf{F}_{[t]} \triangleq \mathbf{H}_{[t]} - \mathbf{M}^T\mathbf{Q}_{[t]}^{-1}\mathbf{P}_{[t]}\mathbf{M}$. From (4), it is clear that all entries in $\mathbf{H}_{[t]}$ (i.e., the Hessian matrix of $f_\mu(\mathbf{y}_{[t]})$) grow to infinity as $\mu \to \infty$. However, from the μ-CS condition, where we have let $\mathbf{p} = \mu\widehat{\mathbf{p}}$ to absorb the μ-factor, we have that $\mathbf{Q}_{[t]}^{-1}\mathbf{P}_{[t]}$ is independent of μ. Also, the matrix $\mathbf{M}$ is determined by network topology and independent of μ. Hence, we have that the term $\mathbf{H}_{[t]}$ dominates $\mathbf{M}^T\mathbf{Q}_{[t]}^{-1}\mathbf{P}_{[t]}\mathbf{M}$ as μ grows to infinity. That is, $\mathbf{F}_{[t]} \to \mathbf{H}_{[t]}$ as $\mu \to \infty$. Also, from the strict convexity of $f_\mu(\cdot)$ and the boundedness of $\mathbf{y}_{[t]}$, we have that $\mathbf{H}_{[t]}$ is positive definite for all t, i.e., $\lambda_{\min}\{\mathbf{H}\} > 0$. Hence, we have $\frac{\lambda_{\min}\{\mathbf{H}\}}{\lambda_{\min}\{\mathbf{F}\}} \to 1$ as $\mu \to \infty$. □

Proof of Theorem 3. The basic idea to prove Theorem 3 is based on analyzing the one-slot drift of the following Lyapunov function: $\hat{V}\left(\mathbf{q}_{[t]}\right) \triangleq \frac{1}{2}\left\|\mathbf{q}_{[t]}\right\|^2$. For convenience, we let $\widehat{\mathbf{y}}_{[t]} \triangleq \left[s_{1,[t]}\cdots s_{F,[t]}, \widehat{x}_{1,[t]}^{(1)}\cdots\widehat{x}_{1,[t]}^{(F)},\cdots,\widehat{x}_{L,[t]}^{(1)}\cdots\widehat{x}_{L,[t]}^{(F)}\right]^T$ group all source and *actual* routing rates. Note that $\widehat{\mathbf{y}}_{[t]} \leq \mathbf{y}_{[t]}$ since $\widehat{x}_{l,[t]}^{(f)} \leq x_{l,[t]}^{(f)}$. Then, the queuing dynamic can be written as $\mathbf{q}_{[t+1]} = \mathbf{q}_{[t]} + \mathbf{M}\widehat{\mathbf{y}}_{[t]}$ and the one-slot drift $\Delta\hat{V}$ can be bounded as:

$$\begin{aligned}\Delta\hat{V} =& \frac{1}{2}\|\mathbf{q}_{[t+1]}\|^2 - \frac{1}{2}\|\mathbf{q}_{[t]}\|^2 = \mathbf{q}_{[t]}^T\mathbf{M}\widehat{\mathbf{y}}_{[t]} + \frac{1}{2}\widehat{\mathbf{y}}_{[t]}^T(\mathbf{M}^T\mathbf{M})\widehat{\mathbf{y}}_{[t]}\\ &\leq \mathbf{q}_{[t]}^T\mathbf{M}\widehat{\mathbf{y}}_{[t]} + \frac{1}{2}\mathbf{y}_{[t]}^T(\mathbf{M}^T\mathbf{M})\mathbf{y}_{[t]}\\ &\overset{(a)}{\leq} \mathbf{q}_{[t]}^T\mathbf{M}\mathbf{y}_{[t]} + NL\max_{\forall l}\{C_l\} + \frac{1}{2}\mathbf{y}_{[t]}^T(\mathbf{M}^T\mathbf{M})\mathbf{y}_{[t]}, \quad (24)\end{aligned}$$

where inequality (a) is due to [3, Lemma 1]. Now, we let $B_4 \triangleq NL\max_{\forall l}\{C_l\} + \frac{1}{2}\lambda_{\max}\{\mathbf{M}^T\mathbf{M}\}\sup_t\{\|\mathbf{y}_{[t]}\|^2\}$. Note that $NL\max_{\forall l}\{C_l\}$ and $\lambda_{\max}\{\mathbf{M}^T\mathbf{M}\}$ are determined by the network topology and $\sup_t\{\|\mathbf{y}_{[t]}\|^2\} \leq (\max\{M, \max_{\forall l} C_l\})^2$. As a result, B_4 depends only on the network and is independent of μ. On the other hand, according to our step-size control in (8) and that $\epsilon = O(\frac{1}{\mu})$, we have $\mathbf{M}\mathbf{y}_{[t]} \leq -\frac{\beta}{\mu}\mathbf{1}$ for some $\beta > 0$. Therefore, we have

$$\begin{aligned}\Delta\hat{V} &\leq \mathbf{q}_{[t]}^T\mathbf{M}\mathbf{y}_{[t]} + B_4 \leq -\frac{\beta}{\mu}\mathbf{q}_{[t]}^T\mathbf{1} + B_4\\ &= -\frac{\beta}{\mu}\sum\nolimits_{f=1}^{F}\sum\nolimits_{n\neq \mathrm{Dst}(f)} q_n^{(f)}[t] + B_4. \quad (25)\end{aligned}$$

So it follows that when $\sum_{f=1}^{F}\sum_{n\neq\mathrm{Dst}(f)} q_n^{(f)}[t] \geq \frac{\mu}{\beta}(B_4 + \epsilon_1)$, where $\epsilon_1 > 0$ is some constant, we have $\Delta\hat{V}(\mathbf{q}_{[t]}) \leq -\epsilon_1$, i.e., the first term in (25) dominates B_4 and results in a negative drift when the total queue length is large.

Next, we claim that the following relationship is true:

$$\limsup_{t\to\infty}\hat{V}(\mathbf{q}_{[t]}) \leq \frac{\mu^2}{2\beta^2}(B_4 + \epsilon_1)^2 + B_4. \quad (26)$$

This claim can be shown by the following argument: First, suppose that $\hat{V}(\mathbf{q}_{[t]}) \leq \frac{\mu^2}{2\beta^2}(B_4 + \epsilon_1)^2$. From (25), we know that $\mathbf{q}_{[t]}^T\mathbf{M}\mathbf{y}_{[t]} \leq 0$, which further implies that $\Delta\hat{V}(\mathbf{q}_{[t]}) < B_4$. As a result, we have

$$\hat{V}(\mathbf{q}_{[t+1]}) = \hat{V}(\mathbf{q}_{[t]}) + \Delta\hat{V}(\mathbf{q}_{[t]}) \leq \frac{\mu^2}{2\beta^2}(B_4 + \epsilon_1)^2 + B_4,$$

i.e., (26) is true. On the other hand, suppose that $\hat{V}(\mathbf{q}_{[t]}) > \frac{\mu^2}{2\beta^2}(B_4 + \epsilon_1)^2$. From the basic relationship between l_1- and l_2-norms, we have $(2\hat{V}(\mathbf{q}_{[t]}))^{\frac{1}{2}} \leq \sum_{f=1}^{F}\sum_{n\neq\mathrm{Dst}(f)} q_n^{(f)}[t]$. This implies that if $\hat{V}(\mathbf{q}_{[t]}) > \frac{\mu^2}{2\beta^2}(B_4 + \epsilon_1)^2$, we have $\Delta\hat{V}(\mathbf{q}_{[t]}) \leq -\epsilon_1$. This means that $\hat{V}(\mathbf{q}_{[t+1]}) < \hat{V}(\mathbf{q}_{[t]})$ and that the sequence $\{\hat{V}(\mathbf{q}_{[t]})\}$ will monotonically decrease at a rate at least ϵ_1. Therefore, there exists a time t' such that $\hat{V}(\mathbf{q}_{[t']}) \leq \frac{\mu^2}{2\beta^2}(B_4 + \epsilon_1)^2$, and then the rest follows from the earlier discussions in the case where $\hat{V}(\mathbf{q}_{[t]}) \leq \frac{\mu^2}{2\beta^2}(B_4 + \epsilon_1)^2$. Finally, we let $K^2 \triangleq 2\left[\frac{\mu^2}{2\beta^2}(B_4 + \epsilon_1)^2 + B_4\right]$ and note that K^2 scales as $O(\mu^2)$. Then, the result stated in the theorem follows by multiplying both sides of (26) by two and taking the square root. This completes the proof. □

So far, we have designed a second-order joint congestion control and routing algorithm and established its utility-optimality and queue-stability. However, given the more complex computational scheme in Algorithm 1, one question begs to be answered: *Can we design a distributed algorithm based on the proposed second-order method?* Moreover, although it is convenient to express (5) and (6) in matrix equations, they are cumbersome to use and more *explicit* scalar-based expressions are desired for implementations in practice. These issues constitute the main discussions in the next section.

V. Second-Order Distributed Algorithm Design

In this section, our main goal is to *decentralize* the proposed second-order method in Section IV. Note that the main computational complexity in (5) and (6) stems from the following two *dense* matrix inverse computations that require global network information:

$$\mathbf{F}_{[t]}^{-1} = \left(\mathbf{H}_{[t]} - \mathbf{M}^T\mathbf{Q}_{[t]}^{-1}\mathbf{P}_{[t]}\mathbf{M}\right)^{-1}, \quad (27)$$

$$\mathbf{G}_{[t]}^{-1} = \left(\mathbf{M}\mathbf{H}_{[t]}^{-1}\mathbf{M}^T - \mathbf{P}_{[t]}^{-1}\mathbf{Q}_{[t]}\right)^{-1}. \quad (28)$$

Thus, our effort in this section is centered around tackling these two challenges. We first derive an alternative way for computing the primal and dual Newton directions in Section V-A. Next, we develop distributed computational schemes for the primal and dual Newton directions in Sections V-B and V-C, respectively.

A. Alternative Computational Scheme for Newton Directions

Our first step towards designing a second-order distributed method is to simplify the computational schemes in (5) and (6). The rationale behind this simplification is due to the following observation: While (5) and (6) "cleanly" express $\mathbf{y}_{[t+1]}$ and $\mathbf{p}_{[t+1]}$ in terms of $\mathbf{y}_{[t]}$ and $\mathbf{p}_{[t]}$ and enable all the subsequent utility-optimality and queue-stability analysis, they also make the computational schemes unnecessarily more complex for practical implementations. Toward this end, we establish the following lemma that will be useful in Sections V-B and V-C:

Lemma 4. *The primal and dual Newton directions in (5) and (6) can be alternatively computed as follows:*

$$\Delta\mathbf{y}_{[t]} = -\mathbf{H}_{[t]}^{-1}\left(\mathbf{g}_{[t]} + \mathbf{M}^T\widetilde{\mathbf{p}}_{[t+1]}\right), \quad (29)$$

$$\Delta\mathbf{p}_{[t]} = \widetilde{\mathbf{p}}_{[t+1]} - \mathbf{p}_{[t]}, \quad (30)$$

where $\widetilde{\mathbf{p}}_{[t+1]}$ is obtained by starting from $\mathbf{p}_{[t]}$ and taking a full Newton step (i.e., $\pi = 1$) and can be computed as:

$$\widetilde{\mathbf{p}}_{[t+1]} = \mathbf{G}_{[t]}^{-1}\left[\mathbf{M}\mathbf{H}_{[t]}^{-1}(-\mathbf{g}_{[t]}) + \mathbf{P}_{[t]}^{-1}\mathbf{1}\right]. \quad (31)$$

The basic idea here is that, through the use of an auxiliary variable $\widetilde{\mathbf{p}}_{[t+1]}$, we obtain simpler expressions in (29) and (30). Clearly, (30) follows from the definition of $\widetilde{\mathbf{p}}_{[t+1]}$. The expressions in (29) and (31) can be derived by solving for $\Delta\mathbf{y}_{[t]}$ and $\Delta\mathbf{p}_{[t]}$ from (18) (changing the indices from "k" to "$[t]$") and replacing $\mathbf{p}_{[t]} + \Delta\mathbf{p}_{[t]}$ by $\widetilde{\mathbf{p}}_{[t+1]}$. With Lemma 4, we are now in a position to derive a distributed scheme for computing primal and dual Newton directions.

B. Distributed Computation of the Primal Newton Direction

The first advantage of using the new scheme in (29) is that, instead of having to deal with $\mathbf{F}_{[t]}$, which is an unstructured and dense matrix, we are now faced with $\mathbf{H}_{[t]}$, which has the following nice *block diagonal* structure:

$$\mathbf{H}_{[t]} = \mathrm{Diag}\left\{\mathbf{S}_{[t]}, \mathbf{X}_{1,[t]}, \ldots, \mathbf{X}_{L,[t]}\right\},$$

where $\mathbf{S}_{[t]} \in \mathbb{R}^{F\times F}$ is a diagonal matrix defined as

$$\mathbf{S}_{[t]} \triangleq \mathrm{Diag}\left\{-\mu U_f''(s_{f,[t]}) + \frac{1}{s_{f,[t]}^2},\ f = 1, \ldots, F\right\}, \quad (32)$$

and where $\mathbf{X}_l \in \mathbb{R}^{F\times F}$ is a symmetric matrix with entries defined as follows:

$$(\mathbf{X}_{l,[t]})_{f_1,f_2} = \begin{cases} \frac{1}{\delta_l^2[t]} + \frac{1}{\left(x_l^{(f_1)}[t]\right)^2} & \text{if } f_1 = f_2, \\ \frac{1}{\delta_l^2[t]} & \text{if } f_1 \neq f_2, \end{cases} \quad (33)$$

where $\delta_l[t] \triangleq C_l - \sum_{f=1}^{F} x_l^{(f)}[t]$ represents the *unused link capacity* of link l in time-slot t. It then follows from the block diagonal structure of $\mathbf{H}_{[t]}$ that

$$\mathbf{H}_{[t]}^{-1} = \mathrm{Diag}\left\{\mathbf{S}_{[t]}^{-1}, \mathbf{X}_{1,[t]}^{-1}, \ldots, \mathbf{X}_{L,[t]}^{-1}\right\}. \quad (34)$$

We note that this block diagonal structure of the Hessian is exactly the same as that in [10, Section V-C] (after replacing the long-term average rates by instantaneous rates in each time-slot t). Due to the same structure as their counterparts in [10], $\mathbf{S}_{[t]}^{-1}$ and $\mathbf{X}_{l,[t]}^{-1}$ can be computed in closed-form by using Lemma 4 and Theorem 5 in [10]. Furthermore, by noting the similarity in structure between (29) and the primal Newton direction scheme in [10, Eq. (9)], we immediately have the following result for second-order congestion control and routing update directions (the proof mirrors that of [10, Theorem 6] and is omitted for brevity):

Theorem 5. *Let $\widehat{\mathbf{x}}_l$ be defined as in [10, Theorem 6]. Given dual prices $\widetilde{\mathbf{p}}_{[t+1]}$, the congestion control and routing directions $\Delta s_{f,[t]}$ and $\Delta x_{l,[t]}^{(f)}$ can be computed in closed-form using local information at each source and each link as follows (omitting time-slot indexes "$[t]$" and "$[t+1]$" for simplicity):*

$$\Delta s_f = \frac{s_f\left(\mu s_f U_f'(s_f) + 1 - s_f\widetilde{p}_{\mathrm{Src}(f)}^{(f)}\right)}{1 - \mu s_f^2 U_f''(s_f)}, \quad \forall f, \quad (35)$$

$$\Delta x_l^{(f)} = \left(x_l^{(f)}\right)^2\Big[\Big(1 - \frac{(x_l^{(f)})^2}{\|\widehat{\mathbf{x}}_l\|^2}\Big)\Big(\frac{1}{x_l^{(f)}} - \frac{1}{\delta_l} + \widetilde{p}_{\mathrm{Tx}(l)}^{(f)} - \widetilde{p}_{\mathrm{Rx}(l)}^{(f)}\Big) + \sum_{f'=1,\neq f}^{F} \frac{(x_l^{(f')})^2}{\|\widehat{\mathbf{x}}_l\|^2}\Big(\frac{1}{x_l^{(f')}} - \frac{1}{\delta_l} + \widetilde{p}_{\mathrm{Tx}(l)}^{(f')} - \widetilde{p}_{\mathrm{Rx}(l)}^{(f')}\Big)\Big],\ \forall l, f. \quad (36)$$

Remark 1. *Theorem 5 has two interesting networking interpretations. First, the dual price differential $(\widetilde{p}_{\mathrm{Tx}(l)}^{(f)} - \widetilde{p}_{\mathrm{Rx}(l)}^{(f)})$ in (36) plays a similar role of the queuing backlog differential in the back-pressure schemes. The main difference is that $\Delta x_l^{(f)}$ (i.e., to increase or decrease $x_{l,[t]}^{(f)}$) is based on not only the pressure differential of session f, but that of all sessions in link l. Moreover, unlike the "winner-take-all" policy in the back-pressure schemes (i.e., the session with the largest backlog differential uses up the link capacity), our second-order approach is more "democratic" in that every session gets a share of the link capacity as indicated in (36).*

C. Distributed Computation of the Dual Newton Direction

Recall that the dual Newton direction $\Delta\mathbf{p}_{[t]}$ can be computed by first solving for $\widetilde{\mathbf{p}}_{[t+1]}$ in (31). However, one technical challenge remains: the term $\mathbf{M}\mathbf{H}_{[t]}^{-1}\mathbf{M}^T$ in $\mathbf{G}_{[t]}$ (cf. (28)) is a *dense* weighted Laplacian matrix [28]. Thus, it is intractable to derive a distributed closed-form expression for $\mathbf{G}_{[t]}^{-1}$. One possible approach to handle this challenge is to borrow the matrix-splitting idea from [9]–[11] to compute $\widetilde{\mathbf{p}}_{[t+1]}$ *iteratively*. This is because the term $\mathbf{P}_{[t]}^{-1}\mathbf{Q}_{[t]}$ in (28) is diagonal and can be absorbed into $\mathbf{M}\mathbf{H}_{[t]}^{-1}\mathbf{M}^T$. Thus, the matrix-splitting scheme in [10], [11] can be adopted with some minor modifications. The most appealing feature of the matrix-splitting scheme is that it only requires *one-hop* information exchange. However, the main drawback of this approach is that the obtained solution is an approximation and only converges to the precise value *asymptotically*. This issue is even more pronounced in a time-slotted system as it entails a *time-scale separation assumption*. To overcome this limitation, in this paper, we propose a *new* iterative approach based on the Sherman-Morrison-Woodbury (SMW) matrix inversion.

Sherman-Morrison-Woodbury matrix inversion approach. The basic idea of the SMW-based approach is that, instead of computing $\mathbf{G}_{[t]}^{-1}$ indirectly by splitting, we *directly* update $\mathbf{G}_{[t]}^{-1}$ using the SMW matrix inversion lemma [7] restated as follows:

Lemma 6 (SMW matrix inversion)**.** *For any invertible matrix $\mathbf{\Omega}$ and vectors $\mathbf{u}, \mathbf{v}$ of conformable dimension, if $1 + \mathbf{v}^T\mathbf{\Omega}^{-1}\mathbf{u} \neq 0$, then $(\mathbf{\Omega} + \mathbf{u}\mathbf{v}^T)^{-1}$ can be computed as:*

$$(\mathbf{\Omega} + \mathbf{u}\mathbf{v}^T)^{-1} = \mathbf{\Omega}^{-1} - \frac{\mathbf{\Omega}^{-1}\mathbf{u}\mathbf{v}^T\mathbf{\Omega}^{-1}}{1 + \mathbf{v}^T\mathbf{\Omega}^{-1}\mathbf{u}}. \quad (37)$$

Note that if $\mathbf{\Omega}^{-1}$ is known and the target matrix can be written as $\mathbf{\Omega}$ coupled with a rank-1 update, then the formula in (37) provides a numerically cheap way to compute the result by a rank-1 correction based on $\mathbf{\Omega}^{-1}$.

In what follows, we outline the key steps of our SMW approach (omitting time-slot index "$[t]$" for simplicity). First, we decompose $\mathbf{G}$ as

$$\mathbf{G} = \big(\mathbf{B}\mathbf{S}^{-1}\mathbf{B}^T - \mathbf{P}^{-1}\mathbf{Q}\big) + \sum_{l=1}^{L} \mathbf{A}_l \mathbf{X}_l^{-1} \mathbf{A}_l^T \qquad (38)$$

using the structures of $\mathbf{M}$ and $\mathbf{H}^{-1}$ (cf. (34)). Note that the term $\mathbf{B}\mathbf{S}^{-1}\mathbf{B}^T - \mathbf{P}^{-1}\mathbf{Q}$ in (38) is diagonal and can be written as:

$$\mathbf{B}\mathbf{S}^{-1}\mathbf{B}^T - \mathbf{P}^{-1}\mathbf{Q} = \mathrm{Diag}\Big\{ \frac{1}{p_n^{(f)}} \Big(\sum_{l\in\mathcal{O}(n)} x_l^{(f)} - \sum_{l\in\mathcal{I}(n)} x_l^{(f)} - s_f \mathbb{1}_f(n) \Big) + \Big(-\mu U_f''(s_f) + \frac{1}{s_f^2} \Big) \mathbb{1}_f(n),\ 1 \le f \le F \Big\}. \qquad (39)$$

We let $\overline{\mathbf{D}} = \mathbf{B}\mathbf{S}^{-1}\mathbf{B}^T - \mathbf{P}^{-1}\mathbf{Q} = \mathrm{Diag}\left\{\overline{\mathbf{D}}_1, \ldots, \overline{\mathbf{D}}_F\right\}$ denote this diagonal matrix. Then, $\overline{\mathbf{D}}^{-1}$ can be readily computed *at each source node* in a distributed fashion.

Next, we note that the term $\sum_{l=1}^{L} \mathbf{A}_l \mathbf{X}_l^{-1} \mathbf{A}_l^T$ in (38) can be further decomposed as:

$$\sum_{l=1}^{L} \mathbf{A}_l \mathbf{X}_l^{-1} \mathbf{A}_l^T = \sum_{l=1}^{L} \Big\{ \mathrm{Diag}\Big\{ x_l^{(f)} \mathbf{a}_l^{(f)} (\mathbf{a}_l^{(f)})^T,\ \forall f \Big\} - \frac{1}{\|\widehat{\mathbf{x}}_l\|^2} \mathbf{u}_l \mathbf{u}_l^T \Big\},$$

where $\mathbf{a}_l^{(f)}$ is as defined in Section IV-A and $\mathbf{u}_l \triangleq \big[(x_l^{(f)})^2 (\mathbf{a}_l^{(f)})^T,\ f = 1, \ldots, F\big]^T$. Note that the first term $\sum_{l=1}^{L} \mathrm{Diag}\{x_l^{(f)} \mathbf{a}_l^{(f)} (\mathbf{a}_l^{(f)})^T,\ \forall f\}$ has exactly the same block-diagonal structure as in $\overline{\mathbf{D}}$. Thus, we can merge it with $\overline{\mathbf{D}}$ to obtain a new block-diagonal matrix $\mathbf{D} = \mathrm{Diag}\left\{\mathbf{D}_1, \ldots, \mathbf{D}_F\right\}$, where each block $\mathbf{D}_f$ is of the form:

$$\mathbf{D}_f = \overline{\mathbf{D}}_f + \sum_{l=1}^{L} (x_l^{(f)})^2 \mathbf{a}_l^{(f)} (\mathbf{a}_l^{(f)})^T. \qquad (40)$$

Now, it is important to recognize from (40) that $\mathbf{D}_f$ can be viewed as *applying rank-1 updates L times* to $\overline{\mathbf{D}}_f$. This motivates us to start from $\overline{\mathbf{D}}_f^{-1}$ and apply the SMW inversion L times to compute $\mathbf{D}_f^{-1}$. Let $\mathbf{D}_{f,[l-1]}^{-1}$ denote the intermediate result before applying the l-th SMW-correction. Also, let $\mathbf{D}_{f,[0]}^{-1} = \overline{\mathbf{D}}_f^{-1}$. Then, we have the following computational scheme based on Lemma 6: For links $l = 1, \ldots, L$,

$$\mathbf{D}_{f,[l]}^{-1} = \mathbf{D}_{f,[l-1]}^{-1} - \frac{\mathbf{D}_{f,[l-1]}^{-1} (x_l^{(f)})^2 \mathbf{a}_l^{(f)} (\mathbf{a}_l^{(f)})^T \mathbf{D}_{f,[l-1]}^{-1}}{1 + (x_l^{(f)})^2 (\mathbf{a}_l^{(f)})^T \mathbf{D}_{f,[l-1]}^{-1} \mathbf{a}_l^{(f)}}. \qquad (41)$$

Clearly, after L times of SMW-corrections, we achieve $\mathbf{D}^{-1} = \mathrm{Diag}\left\{\mathbf{D}_1^{-1}, \ldots, \mathbf{D}_F^{-1}\right\}$. Next, it is important to recognize that

$$\mathbf{G} = \mathbf{D} - \sum_{l=1}^{L} \frac{1}{\|\widehat{\mathbf{x}}_l\|^2} \mathbf{u}_l \mathbf{u}_l^T, \qquad (42)$$

which can be viewed as *applying rank-1 updates L times for* $\mathbf{D}$. Given that $\mathbf{D}^{-1}$ has just been computed, we can apply the SWM inversion lemma another L times to compute $\mathbf{G}^{-1}$ starting from $\mathbf{D}^{-1}$. Toward this end, let $\mathbf{K}_{[l-1]}^{-1}$ denote the intermediate result before applying the l-th SMW-correction. Also, let $\mathbf{K}_{[0]}^{-1} = \mathbf{D}^{-1}$. Then, we have the following computational scheme:

$$\mathbf{K}_{[l]}^{-1} = \mathbf{K}_{[l-1]}^{-1} + \frac{\mathbf{K}_{[l-1]}^{-1} \mathbf{u}_l (\mathbf{u}_l)^T \mathbf{K}_{[l-1]}^{-1}}{\|\widehat{\mathbf{x}}_l\|^2 - (\mathbf{u}_l)^T \mathbf{K}_{[l-1]}^{-1} \mathbf{u}_l},\ l = 1, \ldots, L. \qquad (43)$$

Finally, with the aforementioned $2L$ SMW-corrections in total, we achieve the *precise* value of $\mathbf{G}_{[t]}^{-1}$, which can in turn be used to compute $\widetilde{\mathbf{p}}_{[t+1]}$ and $\Delta\mathbf{p}_{[t]}$. We summarize the SMW-based approach in Algorithm 2.

Algorithm 2 SMW-based approach for dual Newton direction.

Initialization:

1. For each node, compute the corresponding entries in $\overline{\mathbf{D}} = \mathrm{Diag}\left\{\overline{\mathbf{D}}_f, \forall f\right\}$ using (39) and input the result to the starting link.

Main Iteration:

2. For all $f = 1, \ldots, F$, let $\mathbf{D}_{f,[0]}^{-1} = \overline{\mathbf{D}}_f^{-1}$. For links $l = 1, \ldots, L$, update $\mathbf{D}_{f,[l]}$, $\forall f$, using (41). Let $\mathbf{D}^{-1} = \mathrm{Diag}\{\mathbf{D}_{1,[L]}^{-1}, \ldots, \mathbf{D}_{F,[L]}^{-1}\}$.
3. Let $\mathbf{K}_{[0]}^{-1} = \mathbf{D}^{-1}$. For links $l = 1, \ldots, L$, update $\mathbf{K}_{[l]}^{-1}$ using (43). Let $\mathbf{G}_{[t]}^{-1} = \mathbf{K}_{[L]}^{-1}$ and stop.

Remark 2. *Since each SMW-correction only involves information locally available at one link, the scheme can proceed following any pre-determined link ordering in a distributed fashion. Unlike the matrix-splitting approach that converges asymptotically, we require exactly $2L$ SWM-corrections to obtain the precise value of $\mathbf{G}_{[t]}^{-1}$. Thus, the SMW-based approach is far more efficient. However, since the SMW-based approach involves all L links, the scale of information exchange is larger than the 1-hop scale required by the matrix-splitting approach and depends on the network diameter. To see this, without loss of generality, let the links be ordered such that they simply follow the link labels $1, \ldots, L$. Consider the l-th step in (41) or (43), which only requires intermediate result from the $(l-1)$-st step and the local $x_l^{(f)}$-information at link l. In the next step, link l needs to send its computed result to link $l+1$. Consider the extreme case where link l and link $l+1$ are separated from each other by the largest possible number of hops in this network. In this case, it is clear that the required number of hops for sending information from link l to link $l+1$ is equal to the network diameter, i.e., the largest number of hops between any pair of nodes in the network. Fortunately, many communications networks in practice are constructed in a hierarchical fashion such that the network diameter is small.*

VI. Numerical Results

In this section, we conduct numerical studies to verify the efficacy of our proposed second-order joint congestion control and routing algorithm. To illustrate the details of our second-order approach, we first use a small five-node two-session network example as shown in Fig. 5: there are two sessions in the network: N1 to N3 and N4 to N2. Each link in the network has unit capacity. We use $\log(s_f)$ as the utility function, i.e., the well-known proportional fairness metric [29]. We set $\mu = 1000$, meaning that the accuracy

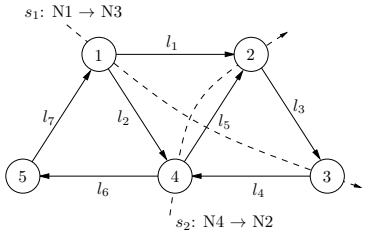

Fig. 5. A five-node two-session network.

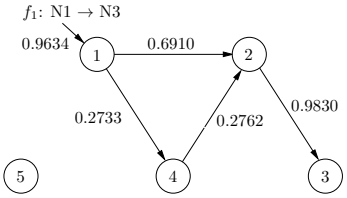

Fig. 6. The routing solutions for session N1 → N3.

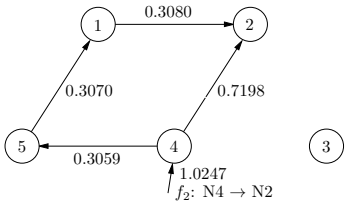

Fig. 7. The routing solutions for session N4 → N2.

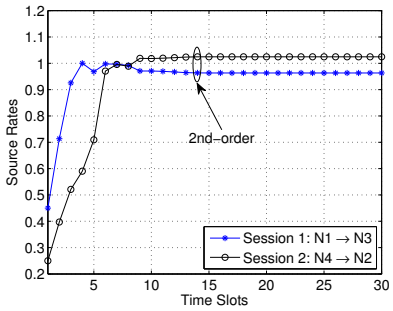

Fig. 8. Convergence process of the second-order algorithm ($\mu = 1000$).

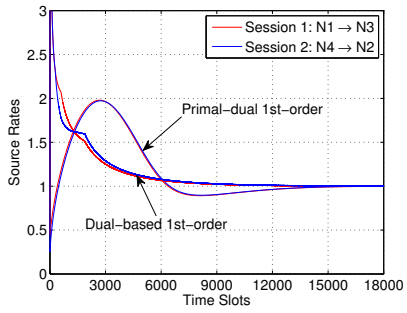

Fig. 9. Convergence process of the first-order methods (V=1000).

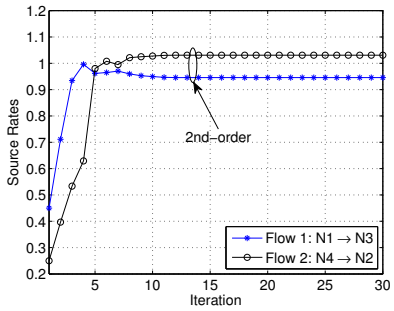

Fig. 10. Convergence process of the second-order algorithm ($\mu = 50$).

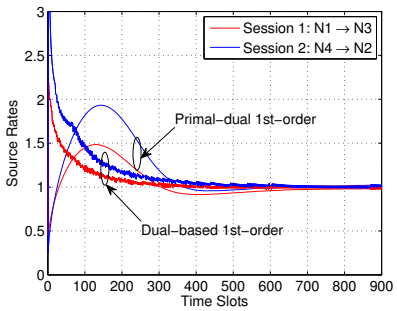

Fig. 11. Convergence process of the first-order methods (V=50).

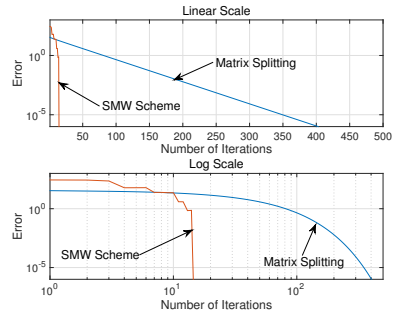

Fig. 12. Performance comparison between the SMW and matrix-splitting inversion schemes.

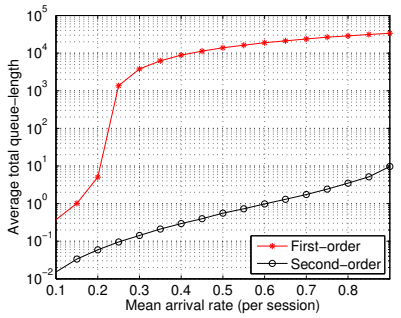

Fig. 13. Average total queue-length vs. mean arrival rate ($\mu = V = 1000$).

of the μ-CS condition is on the order of 10^{-3}. First, the routing solutions for Sessions 1 and 2 are shown in Fig. 6 and Fig. 7, respectively. The convergence behavior is illustrated in Fig. 8. It can be seen from Fig. 8 that the source rates (not just the average source rates) rapidly converge to the following pair $(s_1 = 0.9634, s_2 = 1.0247)$ in approximately 15 iterations. This shows the efficiency of our proposed second-order algorithm.

To compare the convergence performance with the first-order schemes, we also used the same network example in Fig. 5 to experiment with both primal-dual [3] and dual based first-order schemes [1], [2]. For a fair comparison, both first-order back-pressure based schemes were started from the same primal and dual initial points. Targeting approximately the same level of accuracy, we set the step-size scaling factor, denoted as V, as $V = 1000$ (see the discussions in Section IV-B). The convergence performances of both primal-dual and dual based first-order schemes are illustrated in Fig. 9. We can see from Fig. 9 that in order to achieve solutions with high accuracy, both the first-order primal-dual and dual based schemes converge after approximately 15000 iterations. This shows that our second-order scheme converges at least *three orders of magnitude faster* than the first-order schemes. We can also observe that the iterates of the primal-dual based scheme in the first-order domain evolve less abruptly as compared to the dual-based scheme, but also converge more slowly.

To see the impacts of μ and V on the second-order and first-order methods, we let $\mu = 50$, $V = 50$, and run another experiment on the network in Fig. 5. As shown in Fig. 10, we can see that when μ is smaller, our second-order scheme converges even faster (less than 10 iterations) but at the cost of a larger optimality gap. On the other hand, as shown in Fig. 11, with $V = 50$, the convergence of the first-order methods can be made faster (approximately 900 iterations), but this yet exhibits much larger fluctuations. In this case, we can still observe that our second-order scheme converges almost *two orders of magnitude faster* than the first-order schemes. Again, we see that the iterates in the primal-dual based scheme evolve less abruptly with fewer fluctuations, but converge slower. However, regardless of the choice of first-order scheme and the value of V, the evolution of the iterates under both first-order schemes are much less efficient compared to that obtained

under our proposed second-order scheme.

Next, we compare the convergence performance between our proposed SMW-based matrix inversion scheme with the matrix-splitting scheme [9]–[11] in computing dual price updates. For the netwrok example in Fig. 5, the convergence processes of our SMW and the matrix-splitting schemes are illustrated in Fig. 12 (the top and bottom halves are in linear and log scales, respectively). As expected, for this 7-link example, the SWM scheme obtains the *precise* solution in $2\times 7 = 14$ iterations. In contrast, due to its asymptotic nature, matrix-splitting takes over 400 iterations for the approximation error to reach the 10^{-6} precision, which is not very satisfactory even in this small-sized network example.

Lastly, the simulation results of average total queue-lengths vs. mean arrive rates are illustrated in Fig. 13, where we can see that the delay performance of our second-order scheme significantly outperforms that of the first-order methods – more than *three orders* of magnitude lower. This large delay performance gap is a direct consequence of the slow convergence of the first-order methods.

VII. Conclusion

In this paper, we have developed a new second-order algorithmic framework for joint congestion control and routing optimization. Unlike most joint congestion control and routing methods in the literature, our proposed algorithmic framework fundamentally deviates from the classical back-pressure idea to offer not only utility-optimality and queue-stability, but also fast convergence and low delay. Our main contributions in this paper are three-fold: i) We have proposed a second-order joint congestion control and routing framework based on a *primal-dual* interior-point approach that is well-suited for implementation in practice; ii) we have rigorously established the utility-optimality and queue-stability of the proposed second-order joint congestion control and routing framework; and iii) we have proposed several novel approaches for the distributed implementation of our second-order joint congestion control and routing optimization algorithm. Collectively, these results serve as an exciting first step toward an analytical foundation for a second-order joint congestion control and optimization theory that offers fast convergence performance. Second-order cross-layer optimization for network system sis an important and yet under-explored area. Future research topics may include extending and generalizing our proposed second-order algorithmic framework to applications in other network systems, such as wireless networks with stochastic channel models, cloud computing resource allocations, and energy production scheduling in the smart electric power grid.

Appendix A
Proof of Theorem 1

We first show a basic property of the dual sequence $\{\mathbf{p}_{[t]}\}_{t=0}^{\infty}$ that will be useful in proving Theorems 1.

Lemma 7. *For a given μ and under Algorithm 1, if $\|\mathbf{p}_{[0]}\| < \infty$, then $\|\mathbf{p}_{[t]}\| < \infty$ for all t.*

Proof. We prove Lemma 7 result by induction. For $t = 0$, the result is trivially true by assumption. Suppose that at time slot t we have $\|\mathbf{p}_{[t]}\| < B < \infty$; we will show that $\|\mathbf{p}_{[t+1]}\|$ is also bounded. We let $\widetilde{\mathbf{p}}_{[t+1]} \triangleq \mathbf{p}_{[t]} + \Delta\mathbf{p}_{[t]}$, i.e., we let $\pi = 1$. After some algebraic derivations, we have:

$$\widetilde{\mathbf{p}}_{[t+1]} = \left(\mathbf{M}\mathbf{H}_{[t]}^{-1}\mathbf{M}^T - \mathbf{P}_{[t]}^{-1}\mathbf{Q}_{[t]}\right)^{-1}\left[\mathbf{M}\mathbf{H}_{[t]}^{-1}(-\mathbf{g}_{[t]}) + \mathbf{P}_{[t]}^{-1}\mathbf{1}\right].$$

Now, we claim that $\|\widetilde{\mathbf{p}}_{[t+1]}\|$ is bounded. This is true because

$$\begin{aligned}
\|\widetilde{\mathbf{p}}_{[t+1]}\| &\le \left\|\left(\mathbf{M}\mathbf{H}_{[t]}^{-1}\mathbf{M}^T - \mathbf{P}_{[t]}^{-1}\mathbf{Q}_{[t]}\right)^{-1}\left[-\mathbf{M}\mathbf{H}_{[t]}^{-1}\mathbf{g}_{[t]} + \mathbf{P}_{[t]}^{-1}\mathbf{1}\right]\right\| \\
&\overset{(a)}{\le} \left\|(\mathbf{M}\mathbf{H}_{[t]}^{-1}\mathbf{M}^T)^{-1}\left[-\mathbf{M}\mathbf{H}_{[t]}^{-1}\mathbf{g}_{[t]} + \mathbf{P}_{[t]}^{-1}\mathbf{1}\right]\right\| \\
&\overset{(b)}{\le} \lambda_{\min}^{-1}\{\mathbf{M}\mathbf{H}_{[t]}^{-1}\mathbf{M}^T\}\left(\left\|-\mathbf{M}\mathbf{H}_{[t]}^{-1}\mathbf{g}_{[t]}\right\| + \left\|\mathbf{P}_{[t]}^{-1}\mathbf{1}\right\|\right) \\
&\overset{(c)}{\le} \lambda_{\min}^{-1}\{\mathbf{M}\mathbf{H}_{[t]}^{-1}\mathbf{M}^T\}\left(\lambda_{\min}^{-1}\{\mathbf{H}[t]\}\|\mathbf{M}\mathbf{g}_{[t]}\| + \|\mathbf{P}_{[t]}^{-1}\mathbf{1}\|\right), \qquad (44)
\end{aligned}$$

where (a) holds because of the strict feasibility of $\mathbf{y}_{[t]}$ and $\mathbf{p}_{[t]}$ (and hence $-\mathbf{P}_{[t]}^{-1}\mathbf{Q}_{[t]}$ is a positive definite diagonal matrix, which can only increase the eigenvalues of $\mathbf{M}\mathbf{H}_{[t]}^{-1}\mathbf{M}^T$); (b) follows from triangular inequality and taking the smallest eigenvalue of $\mathbf{M}\mathbf{H}_{[t]}^{-1}\mathbf{M}^T$ and factoring it outside the norm; and (c) follows from factoring $\lambda_{\min}^{-1}\{\mathbf{H}[t]\}$ outside the norm. Since $\mathbf{g}_{[t]}$ is continuous, the spectral radius $\rho(\mathbf{H}_{[t]})$ is bounded. Also, since $\mathbf{M}$ is constructed by the NAIM of a connected graph, $\rho(\mathbf{H}_{[t]})$ is also finite. As a result, $\lambda_{\min}^{-1}\{\mathbf{M}\mathbf{H}_{[t]}^{-1}\mathbf{M}^T\}$ must be finite. Also, since $\mathbf{s}_{f,[t]}$ and $\mathbf{x}_l^{(f)}[t]$ are strictly bounded away from zero (due to the step-size selection rule), we have that $\|\mathbf{g}_{[t]}\|$ is bounded. Likewise, since $\mathbf{p}_{[t]}$ is also strictly bounded away from $\mathbf{0}$, we have that $\left\|\mathbf{P}_{[t]}^{-1}\mathbf{1}\right\|$ is bounded from above. Therefore, we can conclude that the RHS of inequality (c) is bounded, i.e., $\|\widetilde{\mathbf{p}}_{[t+1]}\|$ is bounded. Finally, note that $\|\mathbf{p}_{[t+1]}\| = \left\|(1-\pi[t])\mathbf{p}_{[t]} + \pi[t]\widehat{\mathbf{p}}_{[t+1]}\right\| \le (1-\pi[t])\|\mathbf{p}_{[t]}\| + \pi[t]\|\widehat{\mathbf{p}}_{[t+1]}\|$, where the inequality follows again from triangular inequality. Hence, we conclude that $\|\mathbf{p}_{[t+1]}\|$ is also bounded. This completes the proof. □

As mentioned in Section IV-D, the main idea and the key steps for proving Theorem 1 are based on the drift analysis of the following Lyapunov function:

$$V\left(\mathbf{y}_{[t]}, \mathbf{p}_{[t]}\right) \triangleq \frac{1}{2\pi}\left\|\mathbf{y}_{[t]} - \bar{\mathbf{y}}^*\right\|^2 + \frac{1}{2\mu^3\pi}\left\|\mathbf{p}_{[t]} - \mathbf{p}^*\right\|^2,$$

The one-slot drift analysis reveals the following key relationship: $\Delta V\left(\mathbf{y}_{[t]}, \mathbf{p}_{[t]}\right) = V\left(\mathbf{y}_{[t+1]}, \mathbf{p}_{[t+1]}\right) - V\left(\mathbf{y}_{[t]}, \mathbf{p}_{[t]}\right) \le -R\|\mathbf{y}_{[t]} - \bar{\mathbf{y}}^*\| + \frac{1}{\mu}B$, where R and B are both some positive finite quantities independent of μ. Based on this relationship, the result stated in Theorem 1 follows from telescoping T via one-slot drifts and then letting T go to infinity. We begin with evaluating the one-slot Lyapunov drift $\Delta V\left(\mathbf{y}_{[t]}, \mathbf{p}_{[t]}\right)$:

$$\begin{aligned}
\Delta V(\mathbf{y}_{[t]}, \mathbf{p}_{[t]}) &= V(\mathbf{y}_{[t+1]}, \mathbf{p}_{[t+1]}) - V(\mathbf{y}_{[t]}, \mathbf{p}_{[t]}) \\
&= \frac{1}{2\pi}\left(\mathbf{y}_{[t+1]} + \mathbf{y}_{[t]} - 2\bar{\mathbf{y}}^*\right)^T\left(\mathbf{y}_{[t+1]} - \mathbf{y}_{[t]}\right) \qquad (45) \\
&\quad + \frac{1}{2\mu^3\pi}\left(\mathbf{p}_{[t+1]} + \mathbf{p}_{[t]} - 2\mathbf{p}^*\right)^T\left(\mathbf{p}_{[t+1]} - \mathbf{p}_{[t]}\right). \qquad (46)
\end{aligned}$$

In what follows, we will bound the two expressions in (45) and (46) in Appendices A-A and A-B, respectively.

A. One-slot Lyapunov drift of (45)

Note that (45) can be further expanded as:

$$\begin{aligned}(45) &= \Big[\frac{1}{\pi}\left(\mathbf{y}_{[t]}-\bar{\mathbf{y}}^*\right) - \frac{1}{2}\mathbf{F}_{[t]}^{-1}\left(\mathbf{g}_{[t]}-\mathbf{M}^T\mathbf{Q}_{[t]}^{-1}\mathbf{1}\right)\Big]^T \\ &\quad\times\Big[-\pi\mathbf{F}_{[t]}^{-1}\left(\mathbf{g}_{[t]}-\mathbf{M}^T\mathbf{Q}_{[t]}^{-1}\mathbf{1}\right)\Big] \\ &= -\left(\mathbf{y}_{[t]}-\bar{\mathbf{y}}^*\right)^T\mathbf{F}_{[t]}^{-1}\left(\mathbf{g}_{[t]}-\mathbf{M}^T\mathbf{Q}_{[t]}^{-1}\mathbf{1}\right) \quad (47)\\ &\quad+\frac{\pi}{2}\left(\mathbf{g}_{[t]}-\mathbf{M}^T\mathbf{Q}_{[t]}^{-1}\mathbf{1}\right)^T\mathbf{F}_{[t]}^{-2}\left(\mathbf{g}_{[t]}-\mathbf{M}^T\mathbf{Q}_{[t]}^{-1}\mathbf{1}\right). \quad (48)\end{aligned}$$

We first examine (47), which can be computed as follows:

$$\begin{aligned}(47) &= -\left(\mathbf{y}_{[t]}-\bar{\mathbf{y}}^*\right)^T\mathbf{F}_{[t]}^{-1}\left(\mathbf{g}_{[t]}-\mathbf{M}^T\mathbf{Q}_{[t]}^{-1}\mathbf{1}\right)\\ &\overset{(a)}{=} -\left(\mathbf{y}_{[t]}-\bar{\mathbf{y}}^*\right)^T\mathbf{F}_{[t]}^{-1}\left(\mathbf{g}_{[t]}-\mathbf{g}^*-\mathbf{M}^T\mathbf{p}^*-\mathbf{M}^T\mathbf{Q}_{[t]}^{-1}\mathbf{1}\right)\\ &\overset{(b)}{=} -\left(\mathbf{y}_{[t]}-\bar{\mathbf{y}}^*\right)^T\mathbf{F}_{[t]}^{-1}\left(\mathbf{g}_{[t]}-\mathbf{g}^*+\mathbf{M}^T\mathbf{Q}_*^{-1}\mathbf{1}-\mathbf{M}^T\mathbf{Q}_{[t]}^{-1}\mathbf{1}\right)\\ &= -\left(\mathbf{y}_{[t]}-\bar{\mathbf{y}}^*\right)^T\mathbf{F}_{[t]}^{-1}(\mathbf{g}_{[t]}-\mathbf{g}^*) \quad (49)\\ &\quad-\left(\mathbf{y}_{[t]}-\bar{\mathbf{y}}^*\right)^T\mathbf{F}_{[t]}^{-1}\mathbf{M}^T\left(\mathbf{Q}_*^{-1}-\mathbf{Q}_{[t]}^{-1}\right)\mathbf{1}, \quad (50)\end{aligned}$$

where (a) follows from the fact that $\mathbf{g}^*+\mathbf{M}^T\mathbf{p}^*=\mathbf{0}$ (i.e., the μ-ST condition) and (b) follows from the fact that $\mathbf{p}^*=-\mathbf{Q}_*^{-1}\mathbf{1}$ (i.e., the μ-CS condition). Note that the following relationship follows from (49) and the convexity of $\mathbf{f}_\mu(\cdot)$:

$$(49)\le -\frac{1}{\lambda_{\min}\{\mathbf{F}\}}\left(\mathbf{y}_{[t]}-\bar{\mathbf{y}}^*\right)^T\left(\mathbf{g}_{[t]}-\mathbf{g}^*\right). \quad (51)$$

By the Mean-Value Theorem, we have the following pair of relationships:

$$\begin{aligned}f_\mu\left(\mathbf{y}_{[t]}\right) &= f_\mu(\bar{\mathbf{y}}^*)+(\mathbf{g}^*)^T\left(\mathbf{y}_{[t]}-\bar{\mathbf{y}}^*\right)\\ &\quad+\frac{1}{2}\left(\mathbf{y}_{[t]}-\bar{\mathbf{y}}^*\right)^T\mathbf{H}[\widetilde{\mathbf{y}}_1]\left(\mathbf{y}_{[t]}-\bar{\mathbf{y}}^*\right), \quad (52)\\ f_\mu(\bar{\mathbf{y}}^*) &= f_\mu\left(\mathbf{y}_{[t]}\right)+\left(\mathbf{g}_{[t]}\right)^T\left(\bar{\mathbf{y}}^*-\mathbf{y}_{[t]}\right)\\ &\quad+\frac{1}{2}\left(\bar{\mathbf{y}}^*-\mathbf{y}_{[t]}\right)^T\mathbf{H}[\widetilde{\mathbf{y}}_2]\left(\bar{\mathbf{y}}^*-\mathbf{y}_{[t]}\right). \quad (53)\end{aligned}$$

In (52) and (53), $\mathbf{H}[\widetilde{\mathbf{y}}_1]$ and $\mathbf{H}[\widetilde{\mathbf{y}}_2]$ represent the matrices evaluated at points $\widetilde{\mathbf{y}}_1$ and $\widetilde{\mathbf{y}}_2$, where $\widetilde{\mathbf{y}}_1=(1-\alpha_1)\mathbf{y}_{[t]}+\alpha_1\bar{\mathbf{y}}^*$ and $\widetilde{\mathbf{y}}_2=(1-\alpha_2)\mathbf{y}_{[t]}+\alpha_2\bar{\mathbf{y}}^*$, for some $0\le\alpha_1,\alpha_2\le 1$. Next, adding (52) and (53) yields:

$$\begin{aligned}&\left(\mathbf{g}_{[t]}-\mathbf{g}^*\right)^T\left(\mathbf{y}_{[t]}-\bar{\mathbf{y}}^*\right)=\frac{1}{2}\left(\mathbf{y}_{[t]}-\bar{\mathbf{y}}^*\right)^T\times\\ &\left(\mathbf{H}[\widetilde{\mathbf{y}}_1]+\mathbf{H}[\widetilde{\mathbf{y}}_2]\right)\left(\mathbf{y}_{[t]}-\bar{\mathbf{y}}^*\right)\ge\lambda_{\min}(\mathbf{H})\left\|\mathbf{y}_{[t]}-\bar{\mathbf{y}}^*\right\|^2. \quad (54)\end{aligned}$$

Combining (51) and (54), we conclude that

$$(49)\le -R\left\|\mathbf{y}_{[t]}-\bar{\mathbf{y}}^*\right\|^2, \quad (55)$$

where we let $R\triangleq\frac{\lambda_{\min}\{\mathbf{H}\}}{\lambda_{\min}\{\mathbf{F}\}}$. Noting that the μ-factors in $\lambda_{\min}\{\mathbf{H}\}$ and $\lambda_{\min}\{\mathbf{F}\}$ cancel each other, we have that R is independent of μ.

Now, we evaluate the term in (50), which is non-positive because:

$$\begin{aligned}(50) &\le \frac{1}{\lambda_{\min}(\mathbf{F})\Gamma}\left(\mathbf{y}_{[t]}-\bar{\mathbf{y}}^*\right)^T\mathbf{M}^T\mathrm{Diag}\left\{\mathbf{M}\left(\mathbf{y}_{[t]}-\bar{\mathbf{y}}^*\right)\right\}\mathbf{1}\\ &= \frac{1}{\lambda_{\min}(\mathbf{F})\Gamma}\left\|\mathrm{Diag}\left\{\mathbf{M}\left(\mathbf{y}_{[t]}-\bar{\mathbf{y}}^*\right)\right\}\mathbf{1}\right\|^2\le 0, \quad (56)\end{aligned}$$

where Γ is defined as $\Gamma\triangleq\inf_t\{(\sum_{l\in\mathcal{I}(n)}x_{l,[t]}^{(f)}+s_{f,[t]}\mathbb{1}_f(n)-\sum_{l\in\mathcal{O}(n)}x_{l,[t]}^{(f)})(\sum_{l\in\mathcal{I}(n)}\bar{x}_l^{(f),*}+\bar{s}_f^*\mathbb{1}_f(n)-\sum_{l\in\mathcal{O}(n)}\bar{x}_l^{(f,*)})\}$. By combining (55) and (56), we have that

$$(47)\le -R\left\|\mathbf{y}_{[t]}-\bar{\mathbf{y}}^*\right\|^2. \quad (57)$$

Next, by upper-bounding the quadratic term (48), we have:

$$\begin{aligned}(48) &\le \frac{\pi}{2\lambda_{\min}^2\{\mathbf{F}\}}\left\|\mathbf{g}_{[t]}-\mathbf{M}^T\mathbf{Q}_{[t]}^{-1}\mathbf{1}\right\|^2\\ &\overset{(a)}{=}\frac{\pi}{2\lambda_{\min}^2\{\mathbf{F}\}}\left\|\mathbf{g}_{[t]}-\mathbf{g}^*-\mathbf{M}^T\mathbf{p}^*-\mathbf{M}^T\mathbf{Q}_{[t]}^{-1}\mathbf{1}\right\|^2\\ &\overset{(b)}{=}\frac{\pi}{2\lambda_{\min}^2\{\mathbf{F}\}}\left\|\mathbf{g}_{[t]}-\mathbf{g}^*-\mathbf{M}^T\left(\mathbf{Q}_{[t]}^{-1}-\mathbf{Q}_*^{-1}\right)\mathbf{1}\right\|^2\\ &\overset{(c)}{\le}\frac{\pi}{2\lambda_{\min}^2\{\mathbf{F}\}}\left[\left\|\mathbf{g}_{[t]}-\mathbf{g}^*\right\|^2+\left\|\mathbf{M}^T\left(\mathbf{Q}_{[t]}^{-1}-\mathbf{Q}_*^{-1}\right)\mathbf{1}\right\|^2\right], \quad (58)\end{aligned}$$

where inequality (a) utilizes the μ-ST condition $\mathbf{g}^*+\mathbf{M}^T\mathbf{p}^*=\mathbf{0}$ (cf. (13)); equality (b) utilizes the μ-CS condition $\mathbf{p}^*=-\mathbf{Q}_*^{-1}\mathbf{1}$ (cf. (16)); and inequality (c) follows from triangle inequality. Note that the μ-factors in (58) cancel each other. Also, due to the boundedness of $\mathbf{y}_{[t]}$ under the algorithmic design and the assumption that $U_f(\cdot)$ is differentiable, we conclude that (58) is upper-bounded by some constant. By letting

$$B_1\triangleq\frac{1}{2\lambda_{\min}^2\{\mathbf{F}\}}\sup_t\{[\|\mathbf{g}_{[t]}-\mathbf{g}^*\|^2+\|\mathbf{M}^T(\mathbf{Q}_{[t]}^{-1}-\mathbf{Q}_*^{-1})\|^2]\} \quad (59)$$

(cf. B_1 in (23)) and using (57) and (58), we have

$$(45)=(47)+(48)\le -R\left\|\mathbf{y}_{[t]}-\bar{\mathbf{y}}^*\right\|^2+\pi B_1. \quad (60)$$

So far, we have finished the one-slot drift analysis for (45).

B. One-slot Lyapunov drift of (46)

Now, we move on to analyzing the other term (46) in the one-slot drift, which can be further expanded as follows:

$$\begin{aligned}(46) &= -\frac{1}{\mu^3}(\mathbf{p}_{[t]}-\mathbf{p}^*)^T\mathbf{G}_{[t]}^{-1}\Big[\mathbf{M}\mathbf{H}_{[t]}^{-1}\left(\mathbf{g}_{[t]}+\mathbf{M}^T\mathbf{p}_{[t]}\right)\\ &\quad-(\mathbf{Q}_{[t]}+\mathbf{P}_{[t]}^{-1})\mathbf{1}\Big] \quad (61)\\ &\quad+\frac{\pi}{2\mu^3}\Big[\mathbf{M}\mathbf{H}_{[t]}^{-1}\left(\mathbf{g}_{[t]}+\mathbf{M}^T\mathbf{p}_{[t]}\right)-(\mathbf{Q}_{[t]}+\mathbf{P}_{[t]}^{-1})\mathbf{1}\Big]^T\mathbf{G}_{[t]}^{-2}\\ &\quad\times\Big[\mathbf{M}\mathbf{H}_{[t]}^{-1}\left(\mathbf{g}_{[t]}+\mathbf{M}^T\mathbf{p}_{[t]}\right)-(\mathbf{Q}_{[t]}+\mathbf{P}_{[t]}^{-1})\mathbf{1}\Big]. \quad (62)\end{aligned}$$

Note that due to the $\mathbf{H}_{[t]}^{-1}$ term in $\mathbf{G}_{[t]}$, $\mathbf{G}_{[t]}^{-1}$ scales as $O(\mu)$. We first analyze (61), which can be further decomposed as:

$$\begin{aligned}(61) &\overset{(a)}{=} -\frac{1}{\mu^3}(\mathbf{p}_{[t]}-\mathbf{p}^*)^T\mathbf{G}_{[t]}^{-1}\mathbf{M}\mathbf{H}_{[t]}^{-1}(\mathbf{g}_{[t]}-\mathbf{g}^*)\\ &\quad-\frac{1}{\mu^3}(\mathbf{p}_{[t]}-\mathbf{p}^*)^T\mathbf{G}^{-1}\mathbf{M}\mathbf{H}_{[t]}^{-1}\mathbf{M}^T(\mathbf{p}_{[t]}-\mathbf{p}^*)\\ &\quad+\frac{1}{\mu^3}(\mathbf{p}_{[t]}-\mathbf{p}^*)^T\mathbf{G}_{[t]}^{-1}(\mathbf{Q}_{[t]}+\mathbf{P}_{[t]}^{-1})\mathbf{1}\\ &\overset{(b)}{\le} -\frac{1}{\mu^3}(\mathbf{p}_{[t]}-\mathbf{p}^*)^T\mathbf{G}_{[t]}^{-1}\mathbf{M}\mathbf{H}_{[t]}^{-1}(\mathbf{g}_{[t]}-\mathbf{g}^*) \quad (63)\\ &\quad+\frac{1}{\mu^3}(\mathbf{p}_{[t]}-\mathbf{p}^*)^T\mathbf{G}_{[t]}^{-1}(\mathbf{Q}_{[t]}+\mathbf{P}_{[t]}^{-1})\mathbf{1}, \quad (64)\end{aligned}$$

where (a) follows from subtracting the μ-ST condition $\mathbf{g}^* + \mathbf{M}^T\mathbf{p}^* = \mathbf{0}$ and then collecting terms; while (b) holds because $\mathbf{G}_{[t]}^{-1}\mathbf{M}\mathbf{H}_{[t]}^{-1}\mathbf{M}^T$ is positive semidefinite, which implies that $-\frac{1}{\mu^2}\left(\mathbf{p}_{[t]}-\mathbf{p}^*\right)^T\mathbf{G}_{[t]}^{-1}\mathbf{M}\mathbf{H}_{[t]}^{-1}\mathbf{M}^T\left(\mathbf{p}_{[t]}-\mathbf{p}^*\right)\leq 0$. To study the boundedness of (61), we begin with (64), which can be further computed as follows:

$$\begin{aligned}(64) &\overset{(a)}{=}\frac{1}{\mu^3}(\mathbf{p}_{[t]}-\mathbf{p}^*)^T\mathbf{G}_{[t]}^{-1}\left[\mathbf{Q}_{[t]}-\mathbf{Q}_*-\mathbf{P}_*^{-1}+\mathbf{P}_{[t]}^{-1}\right]\mathbf{1}\\ &\overset{(b)}{=}\frac{1}{\mu^3}\left(\mathbf{p}_{[t]}-\mathbf{p}^*\right)^T\mathbf{G}_{[t]}^{-1}\mathbf{M}\left(\mathbf{y}_{[t]}-\mathbf{y}^*\right)\\ &\quad+\frac{1}{\mu^3}\left(\mathbf{p}_{[t]}-\mathbf{p}^*\right)^T\mathbf{G}^{-1}(\mathbf{P}_{[t]}^{-1}-\mathbf{P}_*^{-1})\mathbf{1}\\ &\overset{(c)}{\leq}\frac{1}{\mu^3}\left(\mathbf{p}_{[t]}-\mathbf{p}^*\right)^T\mathbf{G}_{[t]}^{-1}\mathbf{M}\left(\mathbf{y}_{[t]}-\mathbf{y}^*\right),\end{aligned}\tag{65}$$

where equality (a) utilizes the μ-CS condition $\mathbf{Q}_*\mathbf{P}_* = -\mathbf{I}$ (i.e., $\mathbf{Q}_* = -\mathbf{P}_*^{-1}$), equality (b) utilizes $\mathbf{M}\mathbf{y} = \mathbf{Q}\mathbf{1}$, and inequality (c) holds because $\frac{1}{\mu^2}(\mathbf{p}_{[t]}-\mathbf{p}^*)^T\mathbf{G}_{[t]}^{-1}(\mathbf{P}_{[t]}^{-1}-\mathbf{P}_*^{-1})\mathbf{1}\leq -\frac{1}{\mu^2\Phi\lambda_{\min}\{\mathbf{G}_{[t]}\}}(\mathbf{p}_{[t]}-\mathbf{p}^*)^T(\mathbf{p}_{[t]}-\mathbf{p}^*)\leq 0$, where we let $\Phi \triangleq \inf_{t,n,f}\{p_{n,[t]}^{(f)}p_n^{(f),*}\}$. Next, combining (65) with (63), we have

$$(61)\leq\frac{-1}{\mu^3}(\mathbf{p}_{[t]}-\mathbf{p}^*)^T\mathbf{G}_{[t]}^{-1}\mathbf{M}\Big[\mathbf{H}_{[t]}^{-1}(\mathbf{g}_{[t]}-\mathbf{g}^*)-(\mathbf{y}_{[t]}-\bar{\mathbf{y}}^*)\Big].\tag{66}$$

By the vector-valued Taylor expansion of $\mathbf{g}$ [30], we have

$$\mathbf{g}^* = \mathbf{g}_{[t]} + \mathbf{H}_{[t]}\left(\bar{\mathbf{y}}^* - \mathbf{y}_{[t]}\right) + o(\|\mathbf{y}_{[t]}-\bar{\mathbf{y}}^*\|)\mathbf{1},$$

which further implies that

$$\mathbf{H}_{[t]}^{-1}\left(\mathbf{g}_{[t]}-\mathbf{g}^*\right)-\left(\mathbf{y}_{[t]}-\bar{\mathbf{y}}^*\right)=o(\|\mathbf{y}_{[t]}-\bar{\mathbf{y}}^*\|)\mathbf{1}.\tag{67}$$

Therefore, we have

$$\begin{aligned}(66)&\leq\frac{1}{\mu^3}\left(\mathbf{p}_{[t]}-\mathbf{p}^*\right)^T\mathbf{G}_{[t]}^{-1}\mathbf{M}\|\mathbf{y}_{[t]}-\bar{\mathbf{y}}^*\|\mathbf{1}\\ &\overset{(a)}{\leq}\frac{\|\mathbf{y}_{[t]}-\bar{\mathbf{y}}^*\|\|\mathbf{p}_{[t]}-\mathbf{p}^*\|\|\mathbf{M}\mathbf{1}\|}{\mu^3\lambda_{\min}\{\mathbf{G}\}},\end{aligned}\tag{68}$$

where inequality (a) follows from Cauchy-Schwarz inequality. From the boundedness result of $\mathbf{p}$ in Lemma 7, we have that $\|\mathbf{p}_{[t]}-\mathbf{p}^*\|$ is bounded. From our control scheme design, we know that the entries in $\mathbf{y}_{[t]}$ is upper bounded by $\min\{M, C_l, \forall l\}$. Also, it can be shown that $\|\mathbf{M}\mathbf{1}\| = \sum_{f=1}^{F}\sum_{n\neq \mathrm{Dst}(f)}\left|\left|\mathcal{O}(n)\right|-\left|\mathcal{I}(n)\right|+\mathbb{1}_f(n)\right|$, which is a network-specific constant. Hence, we conclude that (68) is upper-bounded by some constant. By letting

$$B_2 \triangleq \frac{\|\mathbf{M}\mathbf{1}\|}{\mu^2\lambda_{\min}\{\mathbf{G}\}}\sup_t\Big\{\left\|\mathbf{y}_{[t]}-\bar{\mathbf{y}}^*\right\|\left\|\mathbf{p}_{[t]}-\mathbf{p}^*\right\|\Big\},\tag{69}$$

(cf. B_2 in (23)) where we leave a μ^2 inside the denominator to cancel out the μ-factors in $\|\mathbf{p}_{[t]}-\mathbf{p}^*\|$ and $\frac{1}{\lambda_{\min}\{\mathbf{G}\}}$, we have $(66)\leq\frac{1}{\mu}B_2$. As a result, we can finally bound (61) as:

$$(61)\leq(63)+(64)\leq(66)\leq\frac{1}{\mu}B_2.\tag{70}$$

Lastly, we evaluate (62). Noting that $\pi\in(0,1]$, we have

$$\begin{aligned}(62)&\leq\frac{1}{2\mu^3}\Big[\mathbf{M}\mathbf{H}_{[t]}^{-1}\left(\mathbf{g}_{[t]}+\mathbf{M}^T\mathbf{p}_{[t]}\right)-(\mathbf{Q}_{[t]}+\mathbf{P}_{[t]}^{-1})\mathbf{1}\Big]^T\mathbf{G}_{[t]}^{-2}\\ &\quad\times\Big[\mathbf{M}\mathbf{H}_{[t]}^{-1}\left(\mathbf{g}_{[t]}+\mathbf{M}^T\mathbf{p}_{[t]}\right)-(\mathbf{Q}_{[t]}+\mathbf{P}_{[t]}^{-1})\mathbf{1}\Big]\\ &\leq\frac{1}{2\mu^3\lambda_{\min}^2\{\mathbf{G}\}}\Big\|\mathbf{M}\mathbf{H}_{[t]}^{-1}\left(\mathbf{g}_{[t]}+\mathbf{M}^T\mathbf{p}_{[t]}\right)-(\mathbf{Q}_{[t]}+\mathbf{P}_{[t]}^{-1})\mathbf{1}\Big\|^2\\ &\overset{(a)}{=}\frac{1}{2\mu^3\lambda_{\min}^2\{\mathbf{G}\}}\Big\|\mathbf{M}\big(\mathbf{H}_{[t]}^{-1}\mathbf{g}_{[t]}-\mathbf{y}_{[t]}\big)+\mathbf{M}\mathbf{H}_{[t]}^{-1}\mathbf{M}^T\mathbf{p}_{[t]}-\mathbf{P}_{[t]}^{-1}\mathbf{1}\Big\|^2\\ &\overset{(b)}{\leq}\frac{1}{2\mu^3\lambda_{\min}^2\{\mathbf{G}\}}\Big[\left\|\mathbf{M}(\mathbf{H}_{[t]}^{-1}\mathbf{g}_{[t]}-\mathbf{y}_{[t]})\right\|+\left\|\mathbf{M}\mathbf{H}_{[t]}^{-1}\mathbf{M}^T\mathbf{p}_{[t]}\right\|\\ &\quad+\left\|\mathbf{P}_{[t]}^{-1}\mathbf{1}\right\|\Big]^2\\ &=\frac{1}{2\mu^3\lambda_{\min}^2\{\mathbf{G}_{[t]}\}}\Big[\left\|\mathbf{M}(\mathbf{H}_{[t]}^{-1}(\mathbf{g}_{[t]}-\mathbf{g}^*)-(\mathbf{y}_{[t]}-\bar{\mathbf{y}}^*))\right.\\ &\quad\left.+\mathbf{M}(\mathbf{H}_{[t]}^{-1}\mathbf{g}^*-\bar{\mathbf{y}}^*)\right\|+\|\mathbf{M}\mathbf{H}_{[t]}^{-1}\mathbf{M}^T\mathbf{p}_{[t]}\|+\|\mathbf{P}_{[t]}^{-1}\mathbf{1}\|\Big]^2\\ &\overset{(c)}{\leq}\frac{1}{2\mu^3\lambda_{\min}^2\{\mathbf{G}\}}\Big[\|\mathbf{y}_{[t]}-\bar{\mathbf{y}}^*\|\|\mathbf{M}\mathbf{1}\|+\|\mathbf{M}(\mathbf{H}_{[t]}^{-1}\mathbf{g}^*-\bar{\mathbf{y}}^*)\|\\ &\quad+\|\mathbf{M}\mathbf{H}_{[t]}^{-1}\mathbf{M}^T\mathbf{p}_{[t]}\|+\|\mathbf{P}_{[t]}^{-1}\mathbf{1}\|\Big]^2,\end{aligned}\tag{71}$$

where (a) uses $\mathbf{Q}_{[t]}\mathbf{1} = \mathbf{M}\mathbf{y}_{[t]}$; (b) is due to the triangular inequality; and (c) follows from the same argument in (67) and (68). Note that in (71), $\|\mathbf{y}_{[t]}-\bar{\mathbf{y}}^*\|\|\mathbf{M}\mathbf{1}\|$ is upper-bounded due to the same argument used for defining B_2; $\|\mathbf{M}(\mathbf{H}_{[t]}^{-1}\mathbf{g}^*-\bar{\mathbf{y}}^*)\|$ is upper-bounded due to the μ-factor cancellation between $\mathbf{H}_{[t]}^{-1}$ and $\mathbf{g}^*$; and $\|\mathbf{M}\mathbf{H}_{[t]}^{-1}\mathbf{M}^T\mathbf{p}_{[t]}\|$ is upper-bounded due to: i) the boundedness of $\|\mathbf{p}_{[t]}\|$ from Lemma 7, and ii) the μ- factor cancellation between $\mathbf{H}_{[t]}^{-1}$ and $\mathbf{p}_{[t]}$. Also, $\|\mathbf{P}_{[t]}^{-1}\mathbf{1}\|$ diminishes as μ increases. Thus, from the above discussions, we conclude that (71) is upper-bounded. By letting

$$\begin{aligned}B_3 \triangleq&\frac{1}{2\mu^2\lambda_{\min}^2\{\mathbf{G}\}}\sup_t\Big\{\Big[\|\mathbf{y}_{[t]}-\bar{\mathbf{y}}^*\|\|\mathbf{M}\mathbf{1}\|\\ &+\|\mathbf{M}(\mathbf{H}_{[t]}^{-1}\mathbf{g}^*-\bar{\mathbf{y}}^*)\|\|\mathbf{M}\mathbf{H}_{[t]}^{-1}\mathbf{M}^T\mathbf{p}_{[t]}\|+\|\mathbf{P}_{[t]}^{-1}\mathbf{1}\|\Big]\Big\},\end{aligned}\tag{72}$$

we have $(62)\leq\frac{1}{\mu}B_3$. Finally, combining this with results in (57), (60), and (70), we arrive at the following result for the one-slot drift analysis:

$$\begin{aligned}&V\left(\mathbf{y}_{[t+1]},\mathbf{p}_{[t+1]}\right)-V\left(\mathbf{y}_{[t]},\mathbf{p}_{[t]}\right)\\ &\qquad\leq-R\|\mathbf{y}_{[t]}-\bar{\mathbf{y}}^*\|^2+\pi B_1+\frac{1}{\mu}B_2+\frac{1}{\mu}B_3.\end{aligned}\tag{73}$$

The remaining steps of the proof include telescoping via T, rearranging, and taking limit over T, and can be found in Section IV-D. This completes the proof of Theorem 1.

REFERENCES

[1] X. Lin and N. B. Shroff, "Joint rate control and scheduling in multihop wireless networks," in *Proc. IEEE CDC*, Atlantis, Paradise Island, Bahamas, Dec. 2006, pp. 1484–1489.

[2] M. J. Neely, E. Modiano, and C.-P. Li, "Fairness and optimal stochastic control for heterogeneous networks," *IEEE/ACM Trans. Netw.*, vol. 16, no. 2, pp. 396–409, Apr. 2008.

[3] A. Eryilmaz and R. Srikant, "Joint congestion control, routing, and MAC for stability and fairness in wireless networks," *IEEE J. Sel. Areas Commun.*, vol. 24, no. 8, pp. 1514–1524, Aug. 2006.

[4] X. Lin and N. B. Shroff, "The impact of imperfect scheduling on cross-layer congestion control in wireless networks," *IEEE/ACM Trans. Netw.*, vol. 14, no. 2, pp. 302–315, Apr. 2006.
[5] A. L. Stolyar, "Maximizing queueing network utility subject to stability: Greedy primal-dual algorithm," *Queueing Systems*, vol. 50, no. 4, pp. 401–457, 2005.
[6] L. Tassiulas and A. Ephremides, "Stability properties of constrained queuing systems and scheduling policies for maximum throughput in multihop radio networks," *IEEE Trans. Autom. Control*, vol. 37, no. 12, pp. 1936–1948, Dec. 1992.
[7] M. S. Bazaraa, H. D. Sherali, and C. M. Shetty, *Nonlinear Programming: Theory and Algorithms*, 3rd ed. New York, NY: John Wiley & Sons Inc., 2006.
[8] A. Eryilmaz and R. Srikant, "Fair resource allocation in wireless networks using queue-length-based scheduling and congestion control," in *Proc. IEEE INFOCOM*, Miami, FL, Mar. 2005, pp. 1804–1814.
[9] E. Wei, A. Ozdaglar, and A. Jadbabaie, "A distributed Newton method for network utitlity maximization," in *Proc. IEEE Conference on Decision and Control (CDC)*, Atlanta, GA, Dec. 15-17, 2010.
[10] J. Liu and H. D. Sherali, "A distributed Newton's method for joint multi-hop routing and flow control: Theory and algorithm," in *Proc. IEEE INFOCOM*, Orlando, FL, Mar. 25-30, 2012, pp. 2489–2497.
[11] J. Liu, C. H. Xia, N. B. Shroff, and H. D. Sherali, "Distributed cross-layer optimization in wireless networks: A second-order approach," in *Proc. IEEE INFOCOM*, Turin, Italy, Apr. 14-19, 2013.
[12] A. Jadbabaie, A. Ozdaglar, and M. Zargham, "A distributed Newton method for network optimization," in *Proc. IEEE Conference on Decision and Control (CDC)*, Shanghai, China, Dec. 16-18, 2009.
[13] A. Forsgren, P. E. Gill, and M. H. Wright, "Interior methods for nonlinear optimization," *SIAM Review*, vol. 44, no. 4, pp. 525–597, Oct. 2002.
[14] M. J. Neely, E. Modiano, and C. E. Rohrs, "Dynamic power allocation and routing for time varying wireless networks," *IEEE J. Sel. Areas Commun.*, vol. 23, no. 1, pp. 89–103, Jan. 2005.
[15] A. Zymnis, N. Trichakis, S. Boyd, and D. OŠNeill, "An interior-point method for large scale network utility maximization," in *Proc. Allerton Conference on Communication, Control, and Computing*, Monticello, IL, Sep. 26-28, 2007.
[16] D. Bickson, Y. Tock, O. Shental, and D. Dolev, "Polynomial linear programming with Gaussian belief propagation," in *Proc. Allerton Conference on Communication, Control, and Computing*, Monticello, IL, Sep. 23-26, 2008, pp. 895–901.
[17] D. Bickson, Y. Tock, A. Zymnis, S. Boyd, and D. Dolev, "Distributed large scale network utility maximization," in *Proc. IEEE International Symposium on Information Theory (ISIT)*, Seoul, Korea, Jun.28–Jul.3, 2009, pp. 829–833.
[18] D. Bickson, "Gaussian belief propagation: Theory and application," Ph.D. dissertation, Hebrew University of Jerusalem, 2009.
[19] E. Wei, A. Ozdaglar, and A. Jadbabaie, "A distributed Newton method for network utility maximization–i: Algorithm," *IEEE Trans. Autom. Control*, vol. 58, no. 9, pp. 2162–2175, Sep. 2013.
[20] S. Boyd and L. Vandenberghe, *Convex Optimization*. Cambridge, UK: Cambridge University Press, 2004.
[21] M. Zargham, A. Ribeiro, and A. Jadbabaie, "Accelerated backpressure algorithm," 2013. [Online]. Available: http://arxiv.org/abs/0704.0217v1
[22] A. Ribeiro, "Stochastic soft backpressure algorithms for routing and scheduling in wireless ad-hoc networks," in *Proc. IEEE CAMSAP*, Aruba, Dutch Antilles, The Netherlands, Dec. 13-16, 2009.
[23] M. Kodialam and T. Nandagopal, "Characterizing achievable rates in multi-hop wireless mesh networks with orthogonal channels," *IEEE/ACM Trans. Netw.*, vol. 13, no. 4, pp. 868–880, 2005.
[24] ——, "Characterizing the capacity region in multi-radio multi-channel wireless mesh networks," in *Proc. ACM Mobicom*, Cologne, Germany, Aug. 2005, pp. 73–87.
[25] M. J. Neely, E. Modiano, and C. E. Rohrs, "Power allocation and routing in multibeam satellites with time-varying channels," *IEEE/ACM Trans. Netw.*, vol. 11, no. 2, pp. 138–152, Feb. 2003.
[26] M. S. Bazaraa, J. J. Jarvis, and H. D. Sherali, *Linear Programming and Network Flows*, 4th ed. New York: John Wiley & Sons Inc., 2010.
[27] A. S. El-Bakry, R. A. Tapia, T. Tsuchiya, and Y. Zhang, "On the formation and theory of the Newton interior-point method for nonlinear programming," *J. Optim. Theory Appl.*, vol. 89, pp. 507–541, 1996.
[28] F. R. K. Chung, *Spectral Graph Theory*. Providence, RI: American Mathematical Society, 1994.
[29] X. Lin, N. B. Shroff, and R. Srikant, "A tutorial on cross-layer optimization in wireless networks," *IEEE J. Sel. Areas Commun.*, vol. 24, no. 8, pp. 1452–1463, Aug. 2006.
[30] W. Rudin, Ed., *Principles of Mathematical Analysis*. New York, NY: McGraw-Hill, 1976.

Jia Liu (S'03–M'10) received his Ph.D. degree in the Bradley Department of Electrical and Computer Engineering at Virginia Tech, Blacksburg, VA in 2010. He is currently a Research Assistant Professor in the Department of Electrical and Computer Engineering at The Ohio State University. His research focus is in the areas of optimization of communication systems and networks, theoretical foundations of cross-layer optimization on wireless networks, design of algorithms, and information theory. Dr. Liu was a Member of Technical Staff at Bell Labs, Lucent Technologies in Beijing China from 1999 to 2003. Dr. Liu is a member of IEEE and SIAM. He is a regular reviewer for major IEEE conferences and journals. He was a recipient of the Bell Labs President Gold Award in 2001, Chinese Government Award for Outstanding Ph.D. Students Abroad in 2008, and the IEEE ICC 2008 Best Paper Award. His received the Best Paper Runner-up Award in IEEE INFOCOM 2011 and the Best Paper Runner-up Award in IEEE INFOCOM 2013. He has served as a TPC member for IEEE INFOCOM since 2010.

Ness B. Shroff (S'91–M'93–SM'01–F'07) received his Ph.D. degree in Electrical Engineering from Columbia University in 1994. He joined Purdue university immediately thereafter as an Assistant Professor in the school of Electrical and Computer Engineering. At Purdue, he became Full Professor of ECE in 2003 and director of CWSA in 2004, a university-wide center on wireless systems and applications. In July 2007, he joined The Ohio State University, where he holds the Ohio Eminent Scholar endowed chair in Networking and Communications, in the departments of ECE and CSE. Dr. Shroff currently serves as editor at large at the IEEE/ACM Trans. on Networking and on the editorial boards of the IEEE Trans. on Control of Network Systems, IEEE Network Magazine, and the Networking Science journal. He has chaired various conferences and workshops, and co-organized workshops for the NSF to chart the future of communication networks. Dr. Shroff is a Fellow of the IEEE and an NSF CAREER awardee. He has received numerous best paper awards for his research. Dr. Shroff is among the list of highly cited researchers from Thomson Reuters ISI and in Thomson Reuters Book on The World's Most Influential Scientific Minds in 2014. He won the IEEE INFOCOM achievement award in 2014.

Cathy H. Xia is an associate professor in the Department of Integrated Systems Engineering at The Ohio State University, with a courtesy appointment from the Department of Computer Science and Engineering. She received her M.S. in Statistics and her Ph.D. in Operations Research, both from Stanford University. Before joining OSU, Dr. Xia had worked at IBM T.J. Watson Research Center as a senior research scientist where she has received numerous IBM research and practice awards. Her areas of research are in performance modeling and analysis, queueing theory and stochastic networks, and distributed optimization with applications in computer networks, information and service systems. She is a co-editor of Springer book "Performance Modeling and Engineering," a co-inventor for more than a dozen US and international patents, and has published over 60 peer-reviewed articles in journals and conference proceedings. She is a recipient of the Best Paper Runner-up Award in IEEE INFOCOM 2013.

Hanif D. Sherali is a University Distinguished Professor Emeritus in the Industrial and Systems Engineering Department at Virginia Polytechnic Institute and State University. His areas of research interest are in mathematical optimization modeling, analysis, and design of algorithms for specially structured linear, nonlinear, and continuous and discrete nonconvex programs, with applications to transportation, location, engineering and network design, production, economics, and energy systems. He has published over 331 refereed articles in various operations research journals and has (co-) authored nine books. He is an elected member of the National Academy of Engineering, a Fellow of both INFORMS and IIE, and a member of the Virginia Academy of Science Engineering and Medicine.